of wave travel times via impulse response functions. Soil Dyn Earthq Eng 21(5):387–404. doi:10.1016/j.soildyn.2007.07.001
55. Todorovska MI, Trifunac MD (2008) Earthquake damage detection in the Imperial County Services Building II: analysis of novelties via wavelets. Struct Control Health Monit (submitted for publication)
56. Todorovska MI, Trifunac MD, Ivanović SS (2001) Wave propagation in a seven-story reinforced concrete building, Part I: theoretical models. Soil Dyn Earthq Eng 21(3):211–223
57. Todorovska MI, Trifunac MD, Ivanović SS (2001) Wave propagation in a seven-story reinforced concrete building, Part II: observed wave numbers. Soil Dyn Earthq Eng 21(3):225–236
58. Trifunac MD (2007) Early History of the Response Spectrum Method, Dept. of Civil Engineering, Report CE 07-01. Univ. Southern California, Los Angeles, California
59. Trifunac MD, Todorovska MI (2001) A note on the useable dynamic range of accelerographs recording translation. Soil Dyn Earthq Eng 21(4):275–286
60. Trifunac MD, Todorovska MI (2001) Evolution of accelerographs, data processing, strong motion arrays and amplitude and spatial resolution in recording strong earthquake motion. Soil Dyn Earthq Eng 21(6):537–555
61. Trifunac MD, Todorovska MI (2001) Recording and interpreting earthquake response of full-scale structures: In Erdik M, Celebi M, Mihailov V, Apaydin N (eds) Proc. of the NATO Advanced Research Workshop on Strong-Motion Instrumentation for Civil Engineering Structures, 2–5 June, 1999. Kluwer, Istanbul, p 24
62. Trifunac MD, Ivanovic SS, Todorovska MI (1999) Experimental evidence for flexibility of a building foundation supported by concrete friction piles. Soil Dyn Earthq Eng 18(3):169–187
63. Trifunac MD, Todorovska MI, Hao TY (2001) Full-scale experimental studies of soil-structure interaction – a review. Proc. of the 2nd US Japan Workshop on Soil-Structure Interaction, 6–8 March, 2001. Tsukuba City, Japan, pp 52
64. Trifunac MD, Ivanović SS, Todorovska MI (2003). Wave propagation in a seven-story reinforced concrete building, Part III: damage detection via changes in wave numbers. Soil Dyn Earthq Eng 23(1):65–75
65. Trifunac MD, Todorovska MI, Manić MI, Bulajić BĐ (2008) Variability of the fixed-base and soil-structure system frequencies of a building – the case of Borik-2 building. Struct Control Health Monit (in press). doi:10.1002/stc.277
66. Udwadia FE, Jerath N (1980) Time variations of structural properties during strong ground shaking. J Eng Mech Div ASCE 106(EM1):111–121
67. Udwadia FE, Marmarelis PZ (1976) The identification of building structural systems I. The linear case. Bull Seism Soc Am 66(1):125–151
68. Udwadia FE, Marmarelis PZ (1976) The identification of building structural systems II. The nonlinear case. Bull Seism Soc Am 66(1):153–171
69. Udwadia FE, Trifunac MD (1974) Time and amplitude dependent response of structures. Earthq Eng Struct Dyn 2:359–378
70. Ward HS, Crawford R (1966) Wind induced vibrations and building modes. Bull Seism Soc Am 56(4):793–813
71. Wong HL, Trifunac MD, Luco JE (1988) A comparison of soil-structure interaction calculations with results of full-scale forced vibration tests. Soil Dyn Earthq Eng 7(1):22–31

Earthquake Early Warning System in Southern Italy

Aldo Zollo[1], Giovanni Iannaccone[2], Vincenzo Convertito[2], Luca Elia[2], Iunio Iervolino[3], Maria Lancieri[2], Anthony Lomax[4], Claudio Martino[1], Claudio Satriano[1], Emanuel Weber[2], Paolo Gasparini[1]

[1] Dipartimento di Scienze Fisiche, Università di Napoli "Federico II" (RISSC-Lab), Napoli, Italy
[2] Osservatorio Vesuviano, Istituto Nazionale di Geofisica e Vulcanologia (RISSC-Lab), Napoli, Italy
[3] Dipartimento di Ingegneria Strutturale, Università di Napoli "Federico II", Napoli, Italy
[4] Alomax Scientific, Mouans-Sartoux, France

Article Outline

Glossary

Data transmission system A multi-component device aimed at the transmission of seismic signals over a distance, also denoted as a telecommunication system. Each data transmission system consists of two basic elements: a transmitter that takes information and converts it to an electromagnetic signal and a receiver that receives the signal and converts it back into usable information.

Modern telecommunication systems are two-way and a single device, a transceiver, acts as both a transmitter and receiver. Transmitted signals can either be analogue or digital. In an analogue signal, the signal is varied continuously with respect to the information. In a digital signal, the information is encoded as a set of discrete, binary values. During transmission, the in-

formation contained in analogue signals will be degraded by noise, while, unless the noise exceeds a certain threshold, the information contained in digital signals will remain intact. This represents a key advantage of digital signals over analogue signals. A collection of transmitters, receivers or transceivers that communicate with each other is a telecommunication network. Digital networks may consist of one or more routers that route data to the correct user.

Earthquake early warning system (EEWS) A real-time, modern information system that is able to provide rapid notification of the potential damaging effects of an impending earthquake, through rapid telemetry and processing of data from dense instrument arrays deployed in the source region of the event of concern (regional EEWS) or surrounding the target infrastructure (site-specific EEWS). A "regional" EEWS is based on a dense sensor network covering a portion or the entirety of an area that is threatened by earthquakes. The relevant source parameters (event location and magnitude) are estimated from the early portion of recorded signals and are used to predict, with a quantified confidence, a ground motion intensity measure at a distant site where a target structure of interest is located. On the other hand, a "site-specific" EEWS consists of a single sensor or an array of sensors deployed in the proximity of the target structure that is to be alerted, and whose measurements of amplitude and predominant period on the initial *P*-wave motion are used to predict the ensuing peak ground motion (mainly related to the arrival of *S* and surface waves) at the same site.

Earthquake location An earthquake location specifies the spatial position and time of occurrence for an earthquake. The location may refer to the earthquake hypocenter and corresponding origin time, a mean or centroid of some spatial or temporal characteristic of the earthquake, or another property of the earthquake that can be spatially and temporally localized.

Earthquake magnitude The magnitude is a parameter used by seismologists to quantify the earthquake size. The Richter magnitude scale, or more correctly, local magnitude ML scale, assigns a single number to quantify the amount of seismic energy released by an earthquake. It is a base-10 logarithmic scale obtained by calculating the logarithm of the combined horizontal amplitude of the largest displacement from zero on a seismometer output. Measurements have no limits and can be either positive or negative.

Introduced by the Japanese seismologist Aki in 1962, the seismic moment is the present-day physical parameter used to characterize the earthquake strength. It represents the scalar moment of one the couples of forces producing the dislocation at an earthquake fault and it is measured from the asymptotic DC level on displacement Fourier spectra of recorded seismic signals.

Probability density function – PDF A function in one or more dimensional space **X** that (i) when integrated over some interval Δx in **X** gives a probability of occurrence of any event within Δx, and (ii) has unit integral over space **X**, where **X** represents a space of possible events.

Seismic data-logger A core element of a digital seismic station, whose aim is to record the analogue signals from seismic sensors and convert them in digital form with an assigned sampling frequency. Ground motion signals acquired by seismic sensors are pre-amplified and anti-aliasing filtered in a data-logger before they are digitalized through an AD (analog-to-digital) converter. The main technical features of a modern data-logger are the number of available channels, the allowed sampling frequencies, the dynamic range, the digitizer clock type, the storage capacity (PCMCIA, internal flash and/or hard disk, USB, . . .), network interfaces (ethernet, wireless lan, or ppp) and power consumption.

Seismic hazard The probability that at a given site, a strong motion parameter (generally the peak ground acceleration) exceeds an assigned value in a fixed time period. When the seismic hazard is computed for an extended region it is generally represented as a map. The hazard map is commonly computed for a constant probability level (10%, 5% or 2%) and a given time window (50 years). It represents the spatial variation of the peak ground acceleration (expressed in percentage of gravity *g*) to be exceeded in the given period with the chosen probability level.

Earthquake early warning systems can provide a mean for the evaluation of real-time hazard maps which evolve with time, as new information about source location, magnitude and predicted peak ground motion parameters are available soon after the earthquake occurrence.

Seismic sensors Instruments used to record the ground vibration produced by natural and artificial sources, generally denoted as seismometers. A seismometer measures the relative motion between its frame and a suspended mass. Early seismometers used optics, or motion-amplifying mechanical linkages. The motion was recorded as scratches on smoked glass, or exposures of light beams on photographic paper. In modern

instruments the proof mass is held motionless by an electronic negative feedback loop that drives a coil. The distance moved, speed and acceleration of the mass are directly measured. Most modern seismometers are broadband, working on a wide range of frequencies (0.01–100 Hz). Another type of seismometer is a digital strong-motion seismometer, or accelerometer, which measures soil acceleration. Due to its relatively high dynamic range, the accelerometer can record unsaturated strong amplitude signals at close distances from a large earthquake. This data is essential to understand how an earthquake affects human structures.

Definition of the Subject

The origin of the term "early warning" probably goes back to the first decades of the last century. However, the first practical use of an "early warning" strategy was military and it was developed during the "cold war" years as a countermeasure to the potential threat from intercontinental ballistic missiles. The objective of these systems was to give an alert to target areas as soon as a missile was detected by a radar system or a launch was detected by a satellite system. In this context the term "lead time" was defined as the time elapsing between the detection of the missile and the estimated impact on the target.

In the last decades the use of the term "early warning" greatly expanded. It is used with small, but significant, variations in various types of risks, from epidemiological, to economic, social, and of course all the types of natural and environmental risks.

In fact, in these contexts, including some natural risks such as hydro-geological and volcanic, the warning is not given at the onset of the catastrophic phenomenon, but after the occurrence of some precursory phenomena which can trigger a catastrophic event (for instance intensive rainfall for hydrological risk, earthquakes and/or ground deformation for volcanic risk). The main consequence of this difference is an increase in the probability of issuing false alarms.

The case of earthquake early warning is similar to missile early warning. The alert is given after an earthquake is detected by a network of seismometers. An earthquake early warning is based on the fact that most of the radiated energy is contained in the slower traveling phases (*S*- and surface waves traveling at about 3.5 km/s or less) which arrive at any location with a delay with respect to small amplitude higher velocity phases (*P*-waves, travelling at about 6–7 km/s) or to an electromagnetically transmitted (EM) signal giving the warning.

Introduction

Many regions in the world are affected by natural hazards such as earthquakes, tsunamis, volcanoes, floods, storms, landslides, etc., each of which can have devastating socio-economic impacts. Among these natural events, earthquakes, have been among the most recurrent and damaging hazards during last few decades, resulting in large numbers of casualties, and massive economic losses [30].

The problem of earthquake risk mitigation is faced using different approaches, depending upon the time scale being considered. Whilst over time scales of decades it is of utmost importance that land use regulations and building/infrastructure codes are continuously updated and improved, for time scales of a few years, the main risk mitigation actions are at the level of information and education in order to increase individual and social community awareness about potentially damaging hazards. Over shorter time scales (months to hours), it would naturally be of great benefit to society as a whole if the capability to accurately predict the time, location and size of a potentially catastrophic natural event were available. However, due to the great complexity of the natural processes of concern, such predictions are currently not possible.

On the other hand, on very short time scales (seconds to minutes), new strategies for earthquake risk mitigation are being conceived and are under development worldwide, based on real-time information about natural events that is provided by advanced monitoring infrastructures, denoted as "early warning systems".

Regional and On-site Early Warning Systems

Earthquake Early Warning Systems (EEWS) are modern, real-time information systems that are able to provide rapid notification of the potential damaging effects of an impending earthquake through the rapid telemetry and processing of data from dense instrument arrays deployed in the source region of the event of concern. Such systems allow mitigating actions to be taken before strong shaking and can significantly shorten the time necessary for emergency response and the recovery of critical facilities such as roads and communication lines.

Advances have been made towards the implementation of operational systems in Japan, Taiwan, and Mexico using two different approaches, i. e., "regional warning" and "onsite warning" [25]. A regional warning system is based on a dense sensor network covering a portion or the entire area that is threatened by earthquakes. The relevant source parameters (earthquake location and magnitude) are estimated from the early portion of recorded signals and are used to predict, with a quantified confidence,

a ground motion intensity measure at a distant site where a target structure of interest is located. Alternatively, "on-site warning" systems consist of a single sensor or an array of sensors deployed in the proximity of the target structure that is to be alerted, and whose measurements on the initial *P*-wave motion are used to predict the ensuing peak ground motion (mainly related to the arrival of *S* and surface waves) at the same site.

Implementation of Early Warning Systems Worldwide

In Japan, since the 1965, the JNR (Japanese National Railway) has developed and operated the Urgent Earthquake Detection and Alarm System (UrEDAS), which is an on-site warning system along the Shinkansen (bullet train) railway. UrEDAS is based on seismic stations deployed along the Japanese Railway with an average distance of 20 km. An alert is issued if the horizontal ground acceleration exceeds 40 cm/s^2. In the 1996, the UrEDAS was combined with a new seismometer called "compact UrEDAS" [31,32,33].

On the other hand, for about one decade the Japanese Meteorological Agency (JMA) has been developing and experimenting with a mixed single station and network based early warning system to generate immediate alerts after earthquakes with JMA Intensity greater than "lower 5" (approximately $M > 6$) [24]. During a testing period from February 2004 to July 2006, the JMA sent out 855 earthquake early warnings, only 26 of which were recognized as false alarms [40]. On October 1, 2007 the broadcast early warning system developed by the Japanese Meteorological Agency (JMA) became operative. In this system, the first warning is issued 2 s after the first *P* phase detection, if the maximum acceleration amplitude exceeds the threshold of 100 cm/s^2.

In the United States the first prototype of an early warning system was proposed by Bakun et al. [4] and developed for mitigating earthquake effects in California. It was designed to rapidly detect the Loma Prieta aftershocks and send an alert when the estimated magnitude was greater than 3.7, in order to reduce the risk of the crews working in the damaged area. The system is composed of four components: ground motion sensors deployed in the epicentral area, a central receiver, radio repeaters and radio receivers. The prototypical system worked for 6 months, during which time 19 events with $M > 3.5$ occurred, 12 alerts were issued with only 2 missed triggers and 1 false alarm.

Based on pioneering work by Allen and Kanamori [2] seismologists across California are currently planning real-time testing of earthquake early warning across the state using the ElarmS (Earthquake Alarms Systems) methodology [1]. The approach uses a network of seismic instruments to detect the first-arriving energy at the surface, the *P*-waves, and translate the information contained in these low amplitude waves into a prediction of the peak ground shaking that follows. Wurman et al. [47] illustrated the first implementation of ElarmS in an automated, non-interactive setting, and the results of 8 months of non-interactive operation in northern California.

Since 1989, in Mexico, the civil association CIRES (Centro de Instrumentacion y REgistro Sismico) with the support of Mexico City Government Authorities, developed and implemented the Mexican Seismic Alert System (SAS) [15]. The SAS is composed of (a) a seismic detection network, 12 digital strong motion stations deployed along 300 km of the Guerrero coast, (b) a dual communication system: a VHF central radio relay station and three UHF radio relay stations, (c) a central control system which continuously controls the operational status of the seismic detection and communication system and, when an event is detected, automatically determines the magnitude and issues the alarm, and (d) a radio warning system for broadcast dissemination of the alarm to end users. After 11 years, the SAS system recorded 1373 events in the Guerrero coast, it issued 12 alerts in Mexico city, with only one false alarm.

In Taiwan, the Taiwan Central Weather Bureau (CWB) developed an early warning system based on a seismic network consisting of 79 strong motion stations installed across Taiwan and covering an area of 100×300 km^2 [44]. Since 1995 the network has been able to report event information (location, size, strong motion map) within 1 min after an earthquake occurrence [39]. To reduce the report time, Wu and Teng [44] introduced the concept of a virtual sub-network: as soon as an event is triggered by at least seven stations, the signals coming from the stations less distant than 60 km from the estimated epicenter are used to characterize the event. This system successfully characterized all the 54 events occurrd during a test period of 7 months (December 2000 – June 2001), with an average reporting time of 22 s.

In Europe, the development and testing of EEWS is being carried out in several active seismic regions. Europe is covered by numerous high-quality seismic networks, managed by national and European agencies, including some local networks specifically designed for seismic early warning around, for example, Bucharest, Cairo, Istanbul and Naples.

In Turkey, an EEWS is operative, called PreSEIS (pre-seismic shaking), to provide rapid alert for Istanbul and surrounding areas. It consists of 10 strong motion sta-

tions located along the border of the Marmara sea along an arc of about 100 km, close to the seismogenetic zone of the Great Marmara Fault Zone with real time data transmission to Kandilli-Oservatory [7,14]. An alarm is issued when a threshold amplitude level is exceeded.

In Romania, the EEWS is based on three tri-axial strong motion sensors deployed in the Vrancea area with a satellite communication link to the Romanian Data Center at NIEP in Bucharest [7,42]. The system is based on first *P* wave detection and prediction of the peak horizontal acceleration recorded in Bucharest, allowing for a warning time of about 25 s.

On 2006 the European Union launched the 3-year project SAFER (Seismic Early Warning for Europe), which is a cooperative scientific program aimed at developing technological and methodological tools that exploit the possibilities offered by real-time analysis of signals coming from these networks for a wide range of actions, performed over time intervals of a few seconds to some tens of minutes. The project includes the participation of 23 research groups from several countries of Europe. The primary aim of SAFER is to develop tools that can be used by disaster management authorities for effective earthquake early warning in Europe and, in particular, its densely populated cities.

The Development of an Early Warning System in Campania Region, Southern Italy

The present article is focused on the description of technologies and methodologies developed for the EEWS under construction in southern Italy.

With about 6 million inhabitants, and a large number of industrial plants, the Campania region (southern Italy), is a zone of high seismic risk, due to a moderate to large magnitude earthquake on active fault systems in the Apenninic belt. The 1980, $M = 6.9$ Irpinia earthquake, the most recent destructive earthquake to occur in the region, caused more than 3000 causalities and major, widespread damage to buildings and infrastructure throughout the region.

In the framework of an ongoing project financed by the Regional Department of Civil Protection, a prototype system for seismic early and post-event warning is being developed and tested, based on a dense, wide dynamic seismic network under installation in the Apenninic belt region (ISNet, Irpinia Seismic Network).

Considering an earthquake warning window ranging from tens of seconds before to hundred of seconds after an earthquake, many public infrastructures and buildings of strategic relevance (hospitals, gas pipelines, railways, railroads, ...) in the Campania region can be considered as potential EEWS target-sites for experimenting with innovative technologies for data acquisition, processing and transmission based on ISNet. The expected time delay to these targets for the first energetic *S* wave train is around 30 s at about 100 km from a crustal earthquake occurring in the source region. The latter is the typical time window available for mitigating earthquake effects through early warning in the city of Naples (about 2 million inhabitants, including suburbs).

This article illustrates the system architecture and operating principles of the EEWS in the Campania region, focusing on its innovative technological and methodological aspects. These are relevant for a reliable real-time estimation of earthquake location and magnitude which are used to predict, with quantified confidence, ground motion intensity at a distant target site.

The system that we describe in this article uses an integrated approach from real time determination of source parameters to estimation of expected losses.

This problem must be dealt in an evolutionary (i. e., time-dependent) and probabilistic framework where probability density functions (PDFs) for earthquake location, magnitude and attenuation parameters are combined to perform a real-time probabilistic seismic hazard analysis.

Earthquake Potential and Seismic Risk in the Campania Region

The southern Apennines are an active tectonic region of Italy that accommodates the differential motions between the Adria and Tyrrhenian microplates [23]. The majority of the seismicity in this region can be ascribed to this motion. These earthquakes mainly occur in a narrow belt along the Apennine chain and are associated with young faults, with lengths ranging from 30 to 50 km, and mainly confined to the upper 20 km of the crust [28,41].

Recent stress and seismic data analyzed by [29] using earthquake locations and fault mechanisms show that the southern Apennines are characterized by an extensional stress regime and normal-fault earthquakes. However, the occurrence of recent (e. g., 5 May, 1990, Potenza, *M* 5.4; 31 October – 1 November, 2002, Molise, M 5.4) and historic (e. g., 5 December, 1456, *M* 6.5) earthquakes do not exclude other mechanisms such as strike-slip faulting.

There have been numerous large and disastrous events in the southern Apennines, including those which occurred in 1694, 1851, 1857 and 1930. The location of historical earthquakes retrieved from the CFTI (Catalogo dei Forti Terremoti in Italia, Catalogue of Strong Earthquakes

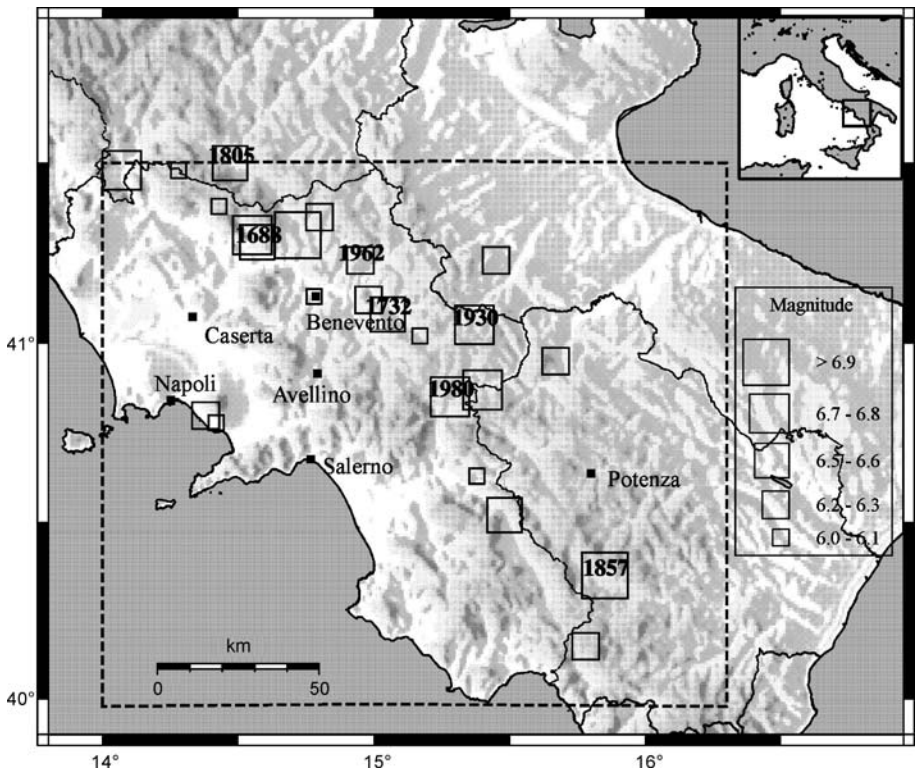

Earthquake Early Warning System in Southern Italy, Figure 1
Location of the main historic earthquakes retrieved from the CFTI database using as region of interest that defined by the external rectangle. The box dimensions are proportional to magnitude. The best constrained historic earthquakes are reported along with their date of occurrence

in Italy) database [6] is shown in Fig. 1. The most recent and well documented event is the complex normal-faulting M 6.9 Irpinia earthquake of 23 November, 1980 [5,43].

As recently indicated in the study by Cinti et al. [9], the southern Apennines has a high earthquake potential with an increasing probability of occurrence for $M \geq 5.5$ earthquakes in the next decade. The new national hazard map (Gruppo di lavoro MPS, 2004), indicates that the main towns of the region fall in a high seismic hazard area, where it is expected that a peak ground acceleration value ranging between 0.15 and 0.25 g will be exceeded in 475 years.

These aspects make the Campania region a suitable experimental site for the implementation and testing of an early warning system. A potential application of an early warning system in the Campania region should consider an expected time delay to the first energetic S wave train varying between 14–20 s at 40–60 km distance to 26–30 s at about 80–100 km, from a crustal earthquake occurring along the Apenninic fault system. Based on those delay times, a large number of civil and strategic infrastructures located in the Campania region are eligible for early waning applications, as shown in Fig. 2.

Seismic Network Architecture and Components

The Irpinia Seismic Network (ISNet) is a local network of strong motion, short period and broadband seismic stations deployed along the southern Apenninic chain covering the seismogenic areas of the main earthquakes that occurred in the region in the last centuries, including the $Ms = 6.9$, 23 November 1980 event.

The seismic network is composed of 29 stations organized in six sub-nets, each of them composed of a maximum of 6–7 stations (Fig. 3). The stations of a given sub-net are connected with real-time communications to a central data-collector site called the Local Control Center (LCC).

The different LCCs are linked to each other and to a Network Control Center (NCC) with different types of transmission systems. The whole data transmission system is fully digital over TCP/IP, from the data-loggers, through

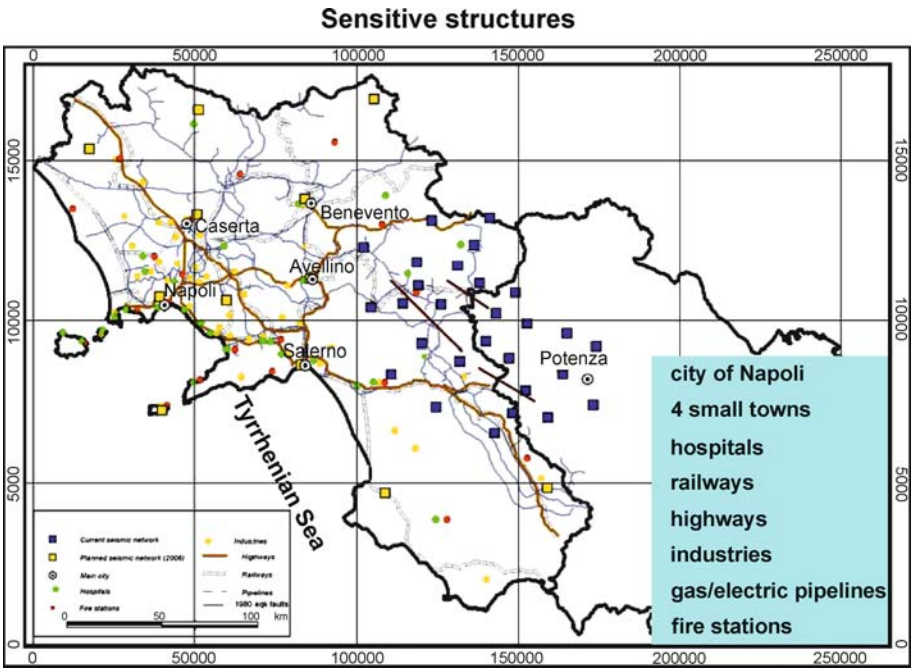

Earthquake Early Warning System in Southern Italy, Figure 2
Distribution of the sensitive structures, potential candidates for an early warning system in the Campania-Lucania region

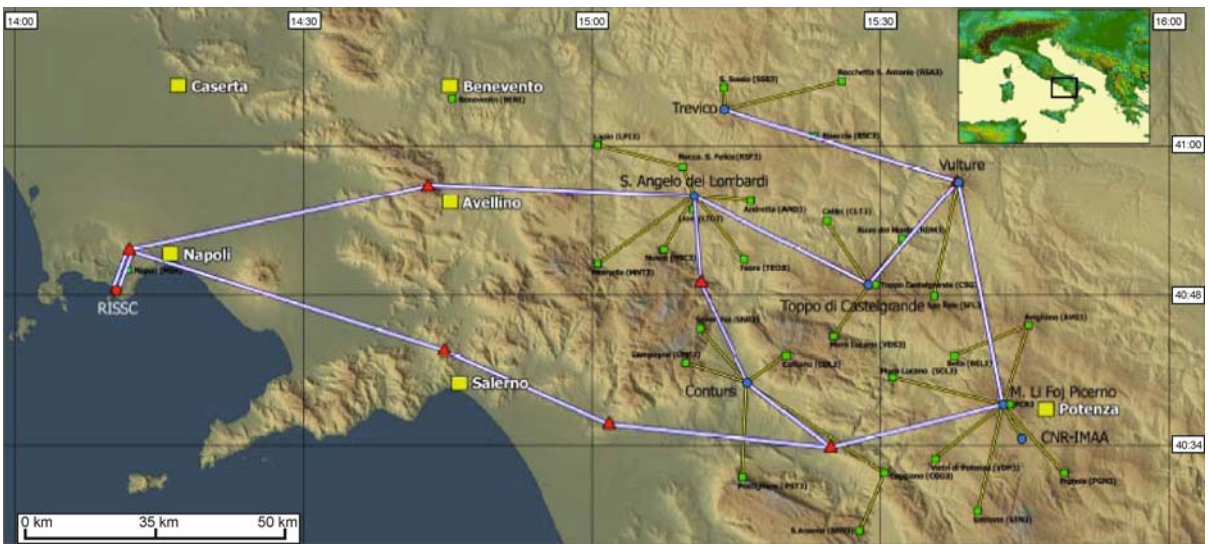

Earthquake Early Warning System in Southern Italy, Figure 3
Topology of the communication system of ISNet showing the extended-star configuration of the seismic network. Symbols explanation: *green squares* – seismic stations; *blue squares* – Local Control Centres (LCC); *yellow lines* – WLAN radio linkconnecting seismic stations and LCC; *white segments* – SDH carrier-class radio; *red triangles* – radio link repeaters; *red circle* – Network Control Centre RISSC in Naples; *yellow squares* – main cities

the LCC, to the NCC, located in the city of Naples, 100 km away from the network center.

To ensure a high dynamic recording range, each seismic station is equipped with a strong-motion accelerometer and a three-component velocity meter (natural period = 1 s). In five station locations the seismometers are replaced by broadband (0.025–50 Hz) sensors to guarantee good-quality recording of teleseismic events. Data ac-

quisition at the seismic stations is performed by the innovative data-logger Osiris-6, produced by Agecodagis sarl. The hardware/software characteristics of the system allow it to install self-developed routines to perform real time specific analysis.

The data-loggers are remotely controlled through a configuration tool accessible via TCP/IP, managing sampling rate, gain, application of calibration signal to the resets of disks, GPS, etc. Furthermore, a complete station health status is available, which helps in the diagnosis of component failure or data-logger malfunction. The data-loggers store the data locally or send it to each LCC where the real-time data management system Earthworm (developed at USGS-United State Geological Survey) is operating.

A calibration unit is installed at each seismic station to automatically provide a periodic calibration signal to seismic sensors in order to verify the correct response curve of the overall acquisition chain.

The power supply of the seismic station is provided by two solar panels (120 W peak, with 480 Wh/day), two 130 Ah gel cell batteries, and a custom switching circuit board between the batteries. With this configuration, 72-h autonomy is ensured for the seismic and radio communication equipment. Each site is also equipped with a GSM/GPRS programmable control/alarm system connected to several environmental sensors and through which the site status is known in real time. With SMS (Short Message Service) and through the programmable GSM controller, the seismic equipment can be completely reset remotely with a power shutdown/restart. The GSM also controls the device start/stop release procedure when the battery goes over/under a predefined voltage level.

Unlike the seismic stations, LCCs, which host the data server and transmission system instruments, are AC power supplied with back-up gel batteries guaranteeing 72-h stand-by power.

Real-Time Data Transmission System

ISNet has a distributed star topology that uses different types of data transmission systems.

The seismic stations are connected via spread-spectrum radio bridges to the LCCs. Data transmission between LCCs from the local control center to the network control center in Naples is performed through different technologies and media types as shown in Table 1.

To transmit waveforms in real time from the seismic stations to the LCCs, a pair of outdoor Wireless LAN bridges operating in the 2.4 GHz ISM band are used. Our tests have shown that these instruments operate continuously without any radio link failure due to adverse weather conditions (snow, heavy rain).

The two primary backbone data communication systems of the central site use Symmetrical High-speed Digital Subscriber Line (SHDSL) technology over a frame-relay protocol. Frame relay offers a number of significant

Earthquake Early Warning System in Southern Italy, Table 1
Specification of the ISNet data communication links

Type	Frequency (GHz)	Bandwidth (Mbps)	# Number of		Comments
			Stations	LCCs	
Spread spectrum Radio	2.45	54	27[3]	–	Throughput around 20–24 Mbps for links between 10–15 km (based on ethernet packets with an average size of 512 bytes).
Ethernet	–	100	2[3]		Stations connected with ethernet cable to LCC infrastructure.
Wireline SHDSL over Frame Relay	–	2.048	–	2	At the central site (RISSC) the CIR[1] is maximum 1.6 Mbps depending upon number of PVCs[2]. At the remote (LCC) site the bandwidth is 640/256 kbps with CIR of 64 kbps in up and download, over ADSL with ATM ABR service class.
Microwave Radio SDH	7	155	–	6	Carrier-class microwave link. Connect six LCC with 155 Mbps (STM-1) truly full bandwidth available. First link constructed for early warning applications.
Microwave Radio HyperLAN/2	5.7	54	–	2	The true usable maximum throughput of HyperLAN/2 is 42 Mbps.

[1] CIR Commited Information Rate.
[2] PVC permanent virtual circuit.
[3] Not included stations hosted by LCCs.

benefits over analogue and digital point-to-point leased lines. With the latter, each LCC requires a dedicated circuit between the LCCs and NCC. Instead, the SHDSL frame relay is a packet-switched network, which allows a site to use a single frame-relay phone circuit to communicate with multiple remote sites through the use of permanent virtual circuits. With virtual circuits, each remote site is seen as part of a single private LAN, simplifying IP address scheme maintenance and station monitoring.

Each seismic site has a real-time data flow of 18.0 kbps (at 125 Hz sampling rate for each physical channel), and the overall data communication bandwidth that is needed is around 540 kbps for 30 stations. ISNet supports this throughput under the worst conditions seen and it has been designed to guarantee further developments, such as the addition of further seismic or environmental sensors, without the need for larger economic and technological investment.

Network Management and Data Archiving

The Network Manager Application and Implementation Overview

As seen in the previous paragraphs, ISNet is a complex infrastructure, and thus needs a suitable software application in order to be effectively managed: a front-end to users and administrators with an interface that is simple to use. To this aim we developed a server-client database-driven application, dubbed *SeismNet Manager*, to keep track of the several components that comprise or are produced by the network, such as stations, devices and recorded data. This application, whose front page is shown in Fig. 4, lets the administrators manage (insert, edit, view and search) the details of (a) seismic stations and Local Control Centers (sites), (b) data communication links between sites (wired or wireless), instruments and devices (sensors, loggers, network hardware), and (c) recorded and computed data (waveforms, events). SeismNet Manager also keeps an

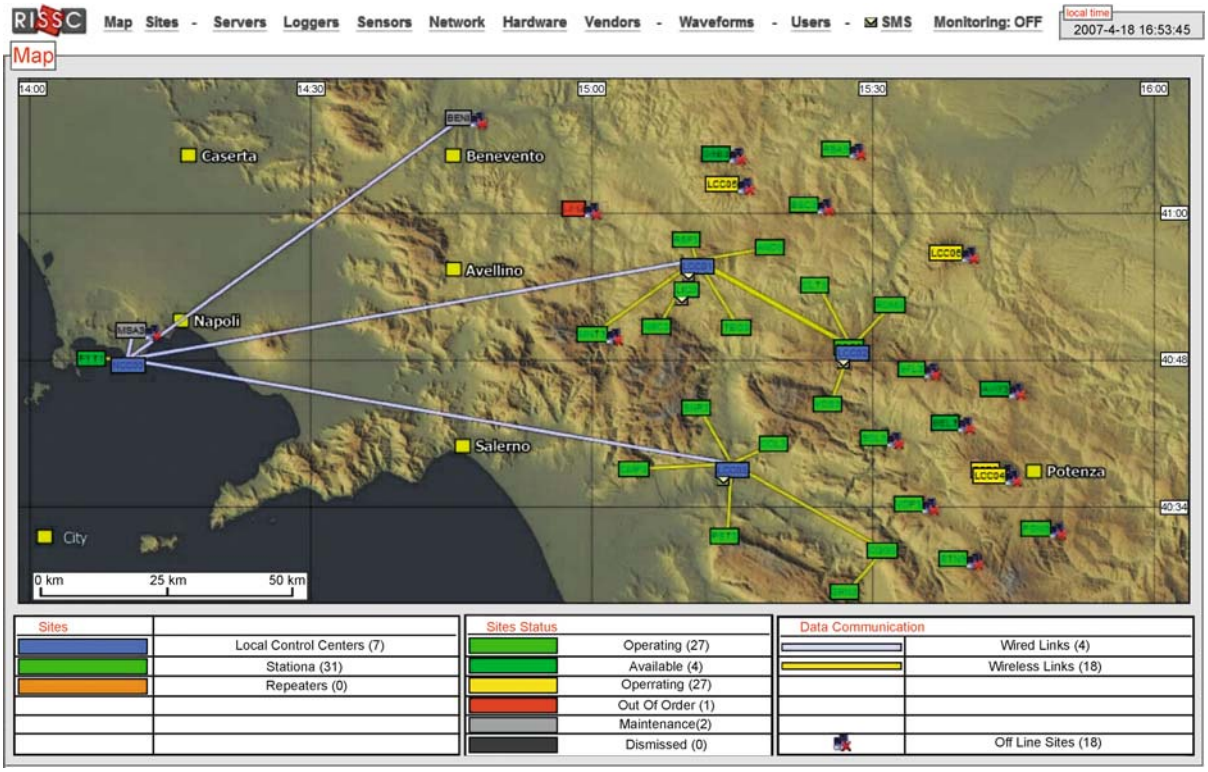

Earthquake Early Warning System in Southern Italy, Figure 4

The front page of SeismNet Devices Manager. This page is meant to convey the state of the whole network at a glance. Each node (station or LCCs) is shown along with its operating state, data links of different types to nearby nodes, whether it's currently on-line or not, along with eventual alarms still pending

historical record of the installations and configurations of the above elements.

All of the mentioned components are handled by leveraging an instrumental database, a flexible repository of information that was implemented by using PostgreSQL, a robust and feature-rich Database Management System available as open source.

The Instrumental Database

The instrumental database is a web-oriented application tool where, at the top level, the network is modeled as a set of sites, with installed loggers, sensors, data acquisition servers, network hardware and generic hardware, in a given configuration. Each of the mentioned entities is mirrored by a different class of objects in the database, where the relevant details are stored and then presented to the users as interactive web pages. As an example, see the page for a typical seismic station in Fig. 5.

The instrumental database was implemented with a layer of abstraction that lets one easily to perform complex queries and hides the actual implementation details of the underlying structure to a possible client. There are both *stored procedures*, i. e., functions that perform complex tasks given simple inputs, and *views*, i. e., virtual database tables that collect the most important pieces of information about an abject, physically scattered in many tables, in a single place and make it possible to easily query,

Earthquake Early Warning System in Southern Italy, Figure 5

The page relative to a seismic station. This page is a collection of all the pieces of information linked to a particular site: location details and map; some pictures and notes; recently received warning messages; currently installed devices and their configurations and mutual connections; data links to other stations; most recent waveforms recorded. Every device at a site also has an associated installation object, that records the configuration parameters and the physical connections to other nearby devices, valid over a period of time. Some elements, such as the data storage servers and the loggers, also need some further configuration parameters, that are independent of their actual physical installation, for things like firmware release and versions of the software packages run

for example, for all the details of the correctly operating sensors installed one year ago at stations with a working wireless link to a given LCC server.

This abstract interface makes the devices database a central repository for effectively cross-correlating the seismic data recorded at any given place and time with the details of the instrument(s) that recorded them, and the configuration details of the systems that ultimately made them available. The interface approach also makes it easier to change the implementation details without the need to update the web application, or any external client procedures that need to interact with the instrumental database.

Automatic Monitoring of the Devices and Automatic Data Retrieval

All of the details about the network described so far are provided by the administrators of the system and are manually updated every time the configuration of something in the network changes, e. g., after installing a new sensor or replacing some faulty hardware at a station. This manual input is needed for "dumb" devices, such as sensors. "Smart" devices, i. e., computers with an IP address (loggers, bridges and Earthworm servers), on the other hand, can be queried about their actual configuration from time to time. The web application can plot the temporal evolution of some selected parameters as graphs, spanning a period ranging from hours to years (Fig. 6). This is useful to correlate issues spotted on the recorded seismic data (typically, "holes" in the stream of data) to hardware problems. It is possible to inspect the whole chain of data transfers to pinpoint the source of the problem (e. g., low batteries on a logger due to a faulty inverter, low signal of a wireless connection due to harsh weather conditions).

There are both automatic and manual procedures to insert new events and data files in the system. The automatic procedures make use of several sources of events to process, such as: INGV (Istituto Nazionale di Geofisica e Vulcanologia, Italy) bi-weekly bulletins; INGV real time alerts; our early warning system. Likewise, they exploit several sources of recorded seismic data in order to provide a SAC file (SAC – seismic analysis code from

Earthquake Early Warning System in Southern Italy, Figure 6

Health graphs of the devices. A device can be marked for monitoring and its internal state, or "health", gets polled at regular intervals. Several of its internal variables are then retrieved and stored into the database, and their temporal evolution can be plotted as a graph. In this case both the internal temperature and CPU load of an OSISRIS data logger are shown, over periods ranging from one hour to one year

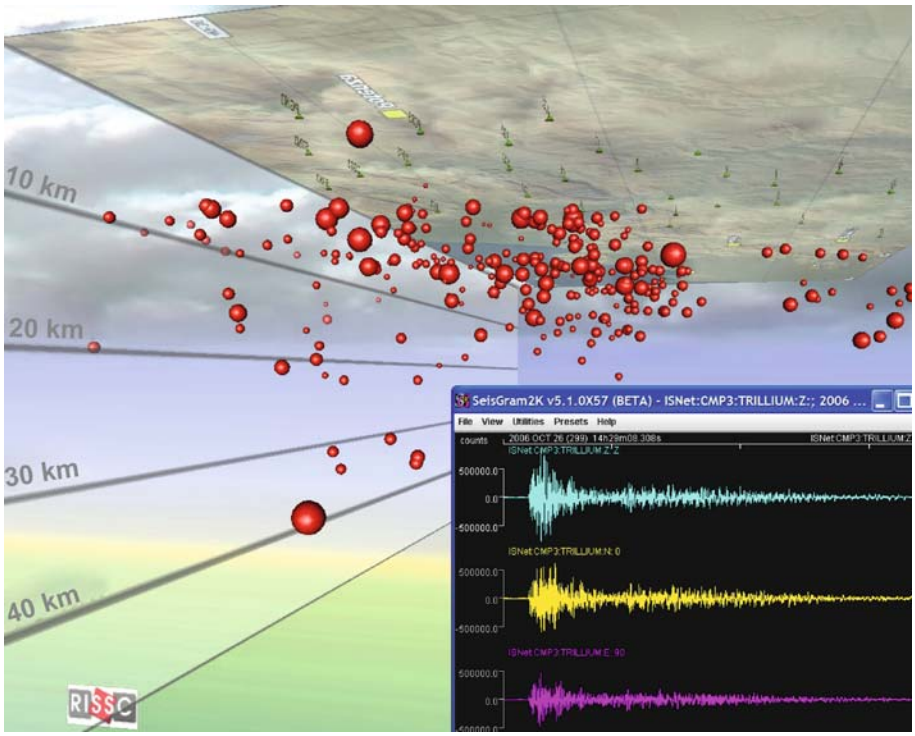

Earthquake Early Warning System in Southern Italy, Figure 7
Visualization of the seismic data. This is the graphical presentation of data recorded by ISNet. The waveforms matching the user's search criteria can be viewed on-line via Seisgram2K (where they can also be processed), while the events are rendered via VRML as a fully interactive 3D scene in the browser itself

Lawrence Livermore National Laboratory) spanning the period from just before the arrival time, up to the end of the event.

Sensor data are retrieved from: (1) a repository of files from the internal mass storage of the loggers; (2) a local Earthworm Wave Server that caches older data collected from all the LCCs; (3) the most recent real time recording from the remote Wave Servers. The instrumental database is used to determine which sites/sensors/configurations recorded each event and to fill the headers of the files using the standard SAC format. The waveforms and events database, on the other end, is used by the automatic procedures to know which pieces of data are still missing for already recorded events (due to e. g., the temporary unavailability of one or more seismic data sources) and need to be collected.

The Waveforms and Events Database: Searching and Visualizing the Seismic Data

We also built a waveform and event database, the natural complement to the instrumental database. It keeps track of the events detected by the network and the relative waveforms recorded by the sensors. This database stores objects for events, origin estimations (time and location), magnitude estimations and waveforms. Several origins can be attached to a single event, as different algorithms and different institutions provide different estimations. Likewise, several magnitude types and estimations are attached to each origin. A waveform object for each sensor that recorded the earthquake is also linked to the event object, and stores a pointer to a SAC file, and its source (site and channel). The latter records are then used to gather, from the instrumental database, the actual details of the instruments that recorded the data.

An interface for searching both events and waveforms is provided, as pictured in Fig. 7. Events can be filtered on origin time and location, magnitude, and distance to the stations. Waveforms can be filtered on station, component, instrument and quality.

Real-Time Earthquake Location and Magnitude Estimation

Real-Time Earthquake Location

Previous Related Studies There are many methodologies for standard earthquake location, performed when

most or all the phase arrival times for an event are available. Standard analysis techniques are generally not suited for early warning applications, since they typically need the seismic event to be fully recorded at several stations, leaving little or no lead time for the warning [25]. For this reason, a different strategy is required, where the computation starts when a few seconds of data and a small number of recording stations are available, and the results are updated with time.

Previous work on earthquake location for early warning includes several approaches to gain constraints on the location at an earlier time and with fewer observations than for standard earthquake location.

In the ElarmS methodology [47], when the first station triggers, the event is temporarily located beneath that station; after a second station trigger the location moves to a point between the two stations, based on the timing of the arrivals; with three or more triggered arrivals, the event location and origin time is estimated using trilateration and a grid search algorithm.

Horiuchi et al. [18] combine standard L2–norm event location, equal differential-time (EDT) location on quasi-hyperbolic surfaces, and the information from not-yet arrived data to constrain the event location beginning when there are triggered arrivals from two stations. The two arrivals times define a hyperbolic surface, which contains the event location. This solution is further constrained by EDT surfaces constructed using the current time (t_{now}) as a substitute for future, unknown arrival times at the stations, which have not yet recorded arrivals. The constraint increases as t_{now} progresses, even if no further stations record an arrival.

Rydelek and Pujol [36], applying the approach of Horiuchi et al. [18], show that useful constraints on an event location can be obtained with only two triggered stations. Cua and Heaton [12], generalized the approach by Rydelek and Pujol in order to start the location with one single triggering station.

The real-time location technique described in this paper is based on the equal differential-time (EDT) formulation [16,27] for standard earthquake location. The EDT location is given by the point traversed by the maximum number of quasi-hyperbolic surfaces, on each of which the difference in calculated travel-time to a pair of stations is equal to the difference in observed arrival times for the two stations. The EDT location determination is independent of origin time and reduces to a 3D search over latitude, longitude and depth. Furthermore, EDT is highly robust in the presence of outliers in the data [27]. This robustness is critical for the problem of earthquake location for seismic early warning, since we will often work with small numbers of data and may have outlier data such as false triggers, picks from other events, and misidentified picks from energetic, secondary phases.

Assuming that a dense seismic network is deployed around the fault zone, we define as the "*evolutionary approach*" a type of analysis where the estimates of earthquake location and size, and their associated uncertainty, evolve with time as a function of the number of recording stations and of the length of the portion of signal recorded at each station.

A direct implication of the evolutionary strategy is that each algorithm must be capable of *real-time* operation, i. e., its computational time must be smaller than the rate at which data enters the system.

Furthermore, since each algorithm starts processing a limited amount of information, the estimated earthquake parameter must be provided, at each time step, as a *probability density function* (PDF) which incorporates in its definition the uncertainties related both to the model employed and to the available data.

The Real-Time Earthquake Location Method The methodology is related to that of Horiuchi et al. [18], which has been extended and generalized by (a) starting the location procedure after only one station has triggered, (b) using the equal differential-time approach proposed by Font [16] to incorporate the triggered arrivals and the not-yet-triggered stations, (c) estimating the hypocenter probabilistically as a PDF instead of as a point, and (d) applying a full, non-linearized, global-search for each update of the location estimate.

We assume that a seismic network has known sets of operational and non-operational stations (Fig. 8a), that when an earthquake occurs, triggers (first *P*-wave arrival picks) will become available from some of the operational stations, and that there may be outlier triggers which are not due to *P* arrivals from the earthquake of interest.

Let's denote the operational stations as $(S_0, \ldots, S_N)$, and consider a gridded search volume V containing the network and target earthquake source regions, and the travel times from each station to each grid point (i, j, k) in V computed for a given velocity model.

The standard EDT approach states that, if the hypocenter (i, j, k) is exactly determined, then the difference between the observed arrival times t_n and t_m at two stations S_n and S_m is equal to the difference between calculated travel times tt_n and tt_m at the hypocentral position, since the observed arrival times share the common earthquake origin time. In other words, the hypocenter must

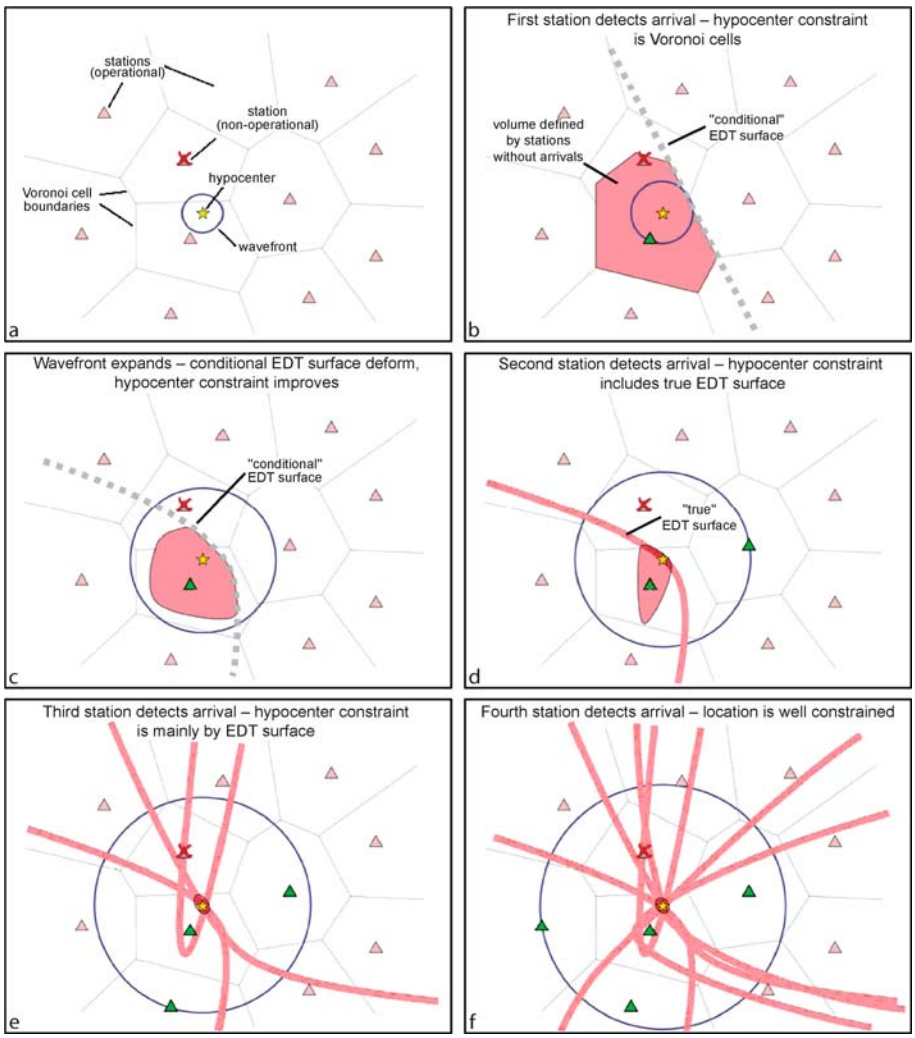

Earthquake Early Warning System in Southern Italy, Figure 8

Schematic illustration of the evolutionary earthquake location algorithm. For clarity, only a map view with the epicentral location is represented. a Given a seismic network with known sets of operational and non-operational stations, we can define a priori the Voronoi cell associated to each station. b When the first station triggers, we can define a volume that is likely to contain the location, this volume is limited by conditional EDT surfaces on which the *P* travel time to the first triggering station is equal to the travel-time to each of the operational but not-yet-triggered stations. c As time progresses, we gain additional information from the stations that have not yet triggered, the EDT surfaces move towards and bend around the first triggering station, and the likely-location volume decreases in size. d When the second station triggers, we can define a true EDT surface; the hypocenter is on the intersection between this surface and the volume defined by the conditional EDT surfaces, which continues decreasing in size. e When a third station triggers, we can define two more true EDT surfaces, further increasing the constraint on hypocenter position. f As more stations trigger, the location converges to the standard EDT location composed entirely of true EDT surfaces

satisfy the equality:

$$(tt_m - tt_n)_{i,j,k} = t_m - t_n \; ; \quad m \neq n \tag{1}$$

for each pair of triggering stations S_n and S_m. For a constant velocity model, this equation defines a 3D hyperbolic surface whose symmetry axis goes through the two stations. Given N triggering stations, $N(N-1)/2$ surfaces can be drawn; the hypocenter is defined as the point crossed by the maximum number of EDT surfaces.

Following an evolutionary approach, the method evaluates, at each time step, the EDT equations considering not only each pair of triggered stations, but also those pairs where only one station has triggered.

Therefore, when the first station, S_n, triggers with an arrival at $t_n = t_{\text{now}}$ (t_{now} is the current clock time), we can already place some limit on the hypocenter position (Fig. 8b). These limits are given by EDT surfaces defined by the condition that each operational but not-yet-triggered station S_l will trigger in the next time instant, $t_l \geq t_n$. That is:

$$(tt_l - tt_n)_{i,j,k} = t_l - t_n \geq 0\,; \quad l \neq n\,. \tag{2}$$

On these conditional EDT surfaces, the P travel time to the first triggering station tt_n is equal to the travel-time to each of the not-yet-triggered stations, tt_l, $l \neq n$. These surfaces bound a volume (defined by the system of inequalities) which must contain the hypocenter. In the case of a homogeneous medium with constant P-wave speed, this hypocentral volume is the Voronoi cell around the first recording station, defined by the perpendicular bisector surfaces with each of the immediate neighboring stations.

As the current time t_{now} progresses, we gain the additional information that the not-yet-triggered stations can only trigger with $t_l > t_{\text{now}}$. Thus the hypocentral volume is bounded by conditional EDT surfaces that satisfy the inequality:

$$(tt_l - tt_n)_{i,j,k} \geq \delta t_{n,l}\,; \quad l \neq n\,. \tag{3}$$

δt is the time interval between the arrival time at station S_n and the latest time for which we have information from station S_l,

$$\delta t_{n,l} = t_{\text{now}} - t_n\,, \tag{4}$$

where t_n is the observed arrival time at station S_n.

The system (3) defines the volume, bounded by the conditional EDT surfaces, in which the hypocenter may be located given that, at current time t_{now}, only the station S_n has triggered. When $\delta t = 0$ the system (3) reduces to the system (2); for $\delta t > 0$, the hypocentral volume will be smaller than the previous one, since the updated, conditional EDT surfaces tend to fold towards and around the first triggered station (Fig. 8c).

We interpret the hypocentral volume in a probabilistic way by defining, for each inequality in (3), a value $p_{n,l}(i, j, k)$ which is 1 if the inequality is satisfied and 0 if not. Then we sum the $p_{n,l}(i, j, k)$ over stations l at each grid point, obtaining a non-normalized probability density $P(i, j, k)$, where $P(i, j, k) = N - 1$ for grid points where all the inequalities are satisfied and a value less than $N - 1$ elsewhere.

When the second and later stations trigger, we first re-evaluate the system (3) for all pairs of triggered stations S_n and all not-yet-triggered stations S_l. Secondly, we construct standard, true EDT surfaces (see Eq. 2) between each pair S_n, S_m of the triggered stations, by evaluating for each grid point the quantity:

$$q_{n,m}(i, j, k) = \exp\left\{-\frac{[(tt_n - tt_m)_{i,j,k} - (t_n - t_m)]^2}{2\sigma^2}\right\}\,; \quad n \neq m\,. \tag{5}$$

The expression between square brackets at the exponent is the standard EDT Eq. 2 whose solutions are quasi-hyperbolic surfaces; in practice all true EDT surfaces are given a finite width by including the uncertainty σ in the arrival time picking and the travel-time calculation.

The quantity $q_{n,m}(i, j, k)$ has values between 0 and 1. We sum the $q_{n,m}(i, j, k)$ with the $p_{n,l}(i, j, k)$ obtained from the re-evaluation of (4) to obtain a new $P(i, j, k)$.

Starting from P, we define a value:

$$Q(i, j, k) = \left(\frac{P(i, j, k)}{P_{\max}}\right)^N\,, \tag{6}$$

which forms a relative probability density function (PDF, with values between 0 and 1) for the hypocenter location within the grid cell (i, j, k). The function $Q(i, j, k)$ may be arbitrarily irregular and may have multiple maxima.

At predetermined time intervals, we evaluate (3) and (5) to obtain $Q(i, j, k)$ in the search volume, using the Oct-tree importance sampling algorithm ([13,27], http://www.alomax.net/nlloc/octtree). This algorithm uses recursive subdivision and sampling of rectangular cells in 3D space to generate a cascade structure of sampled cells, such that the spatial density of sampled cells follows the target function values. The Oct-tree search is much faster than a simple or nested grid search (factor 10–100 faster) and more global and complete than stochastic search methods algorithms such as simulated annealing and genetic algorithms [13]. For each grid point, an origin time estimate can be obtained from the observed arrival times and the calculated travel times.

As more stations trigger, the number of not-yet-triggered stations becomes small, and the location converges towards the hypocentral volume that is obtained with standard EDT location using the full set of data from all operational stations (Fig. 8d–f).

If there are uncorrelated outlier data (i. e., triggers that are not compatible with P arrivals from a hypocenter within or near the network), then the final hypocentral volume will usually give an unbiased estimate of the hypocentral location, as with standard EDT location.

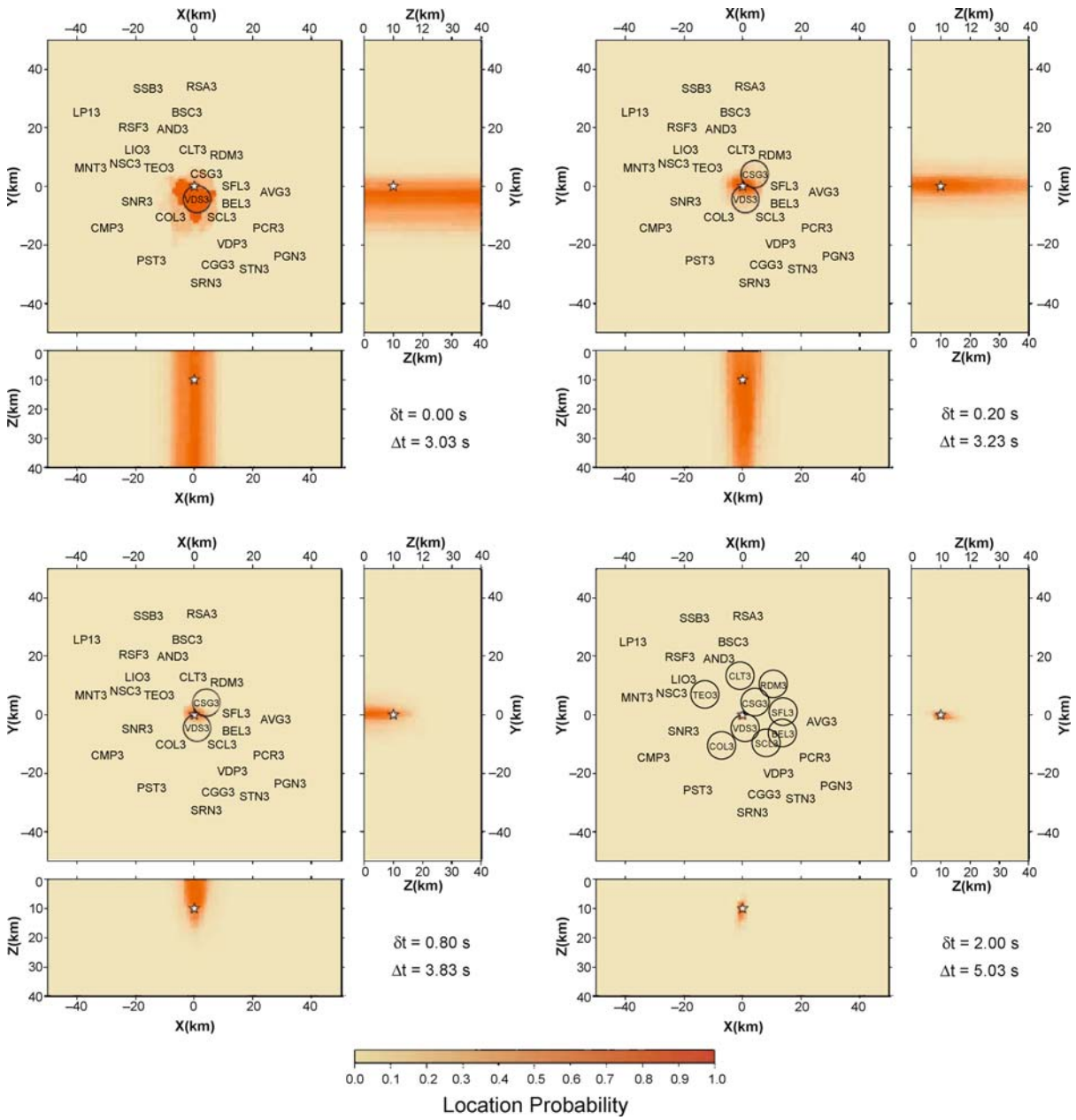

Earthquake Early Warning System in Southern Italy, Figure 9

Location test for a synthetic event occurring at the center of the Irpinia Seismic Network (ISNet). The three orthogonal views show marginal values of the probability function $Q(i, j, k)$. The true hypocenter is identified by a *star*. δt is the time from the first trigger, Δt is the time from event origin. For each snapshot, stations that have triggered are marked with a *circle*

However, if one or more of the first arrival times is an outlier, then the earliest estimates of the hypocentral volume may be biased. Synthetic tests have shown that, if N_{out} is the number of outlier data, the bias reduces significantly after about $4 + N_{\text{out}}$ arrivals have been obtained, and then decreases further with further arrivals, as the solution converges towards a standard EDT location [37].

We performed several synthetic tests using the geometry of the ISNet network. For each simulated event, we computed theoretical arrival picks using travel times ob-

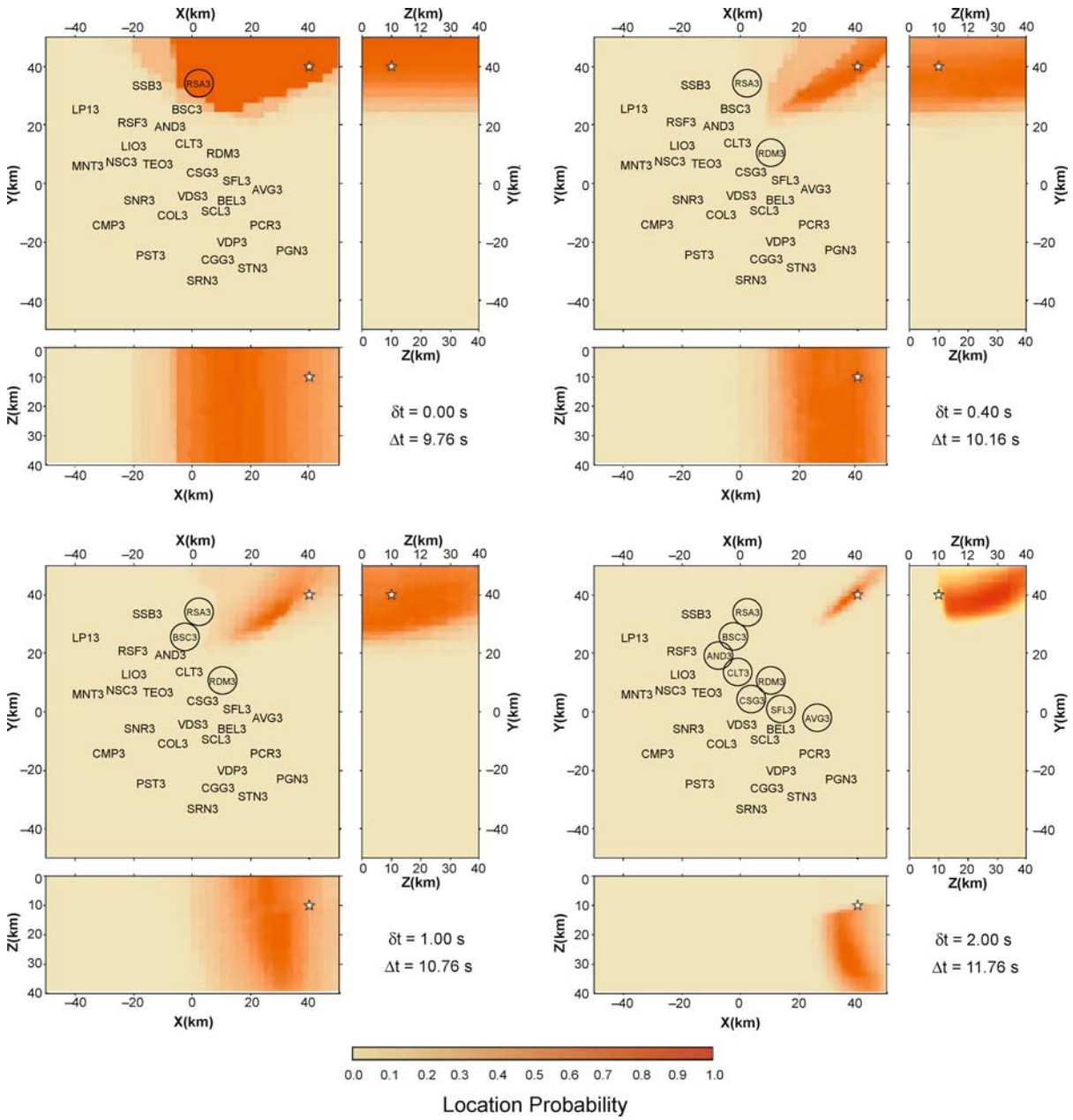

Earthquake Early Warning System in Southern Italy, Figure 10
Location test for a synthetic event occurring outside the ISNet network (see Fig. 9 for explanation)

tained by the finite difference solution of the eikonal equation [35] for a 1D, *P*-wave velocity model. To reproduce uncertainties introduced by the picking algorithm, we add to each arrival time a random error following a Gaussian distribution with a variance of 0.02 s.

Here we use only *P* picks since currently most networks have poor capability to perform real-time *S* picking. Our tests consider an earthquake occurring at the center of the network at a depth of 10 km (Fig. 9) and an earthquake occurring outside the network at a depth of 10 km (Fig. 10). Each panel in Figs. 9 and 10 is a snapshot at a given time showing the marginal map (i. e., summed over i, j or k) for $Q(i, j, k)$ along the horizontal (x, y) and the two vertical (x, z and y, z) planes. The star shows the

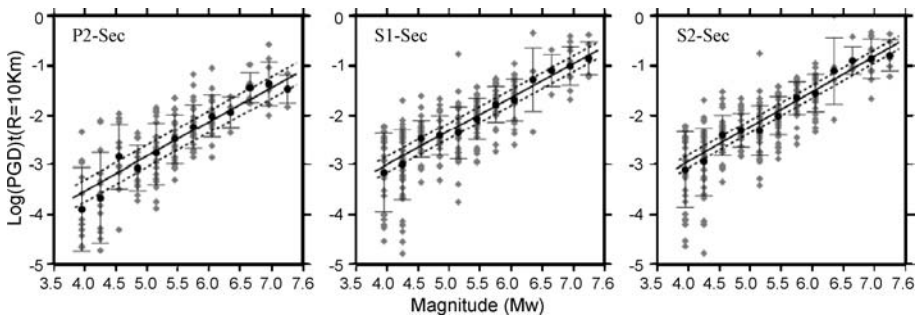

Earthquake Early Warning System in Southern Italy, Figure 11
Correlation between low-pass filtered peak ground motion value and moment-magnitude for earthquakes occurred in the Euro-Mediterranean region (after [49]). The panels show the logarithm of peak ground displacement normalized at a reference distance of 10 km as a function of Mw in time windows of (*left*) 2 s length from the first *P*-arrival and (*middle*) 1- and (*right*) 2-s from the first *S*-arrivals. *P*- and *S*-data are measured on vertical and root-squared sum of horizontal components, respectively. Each panel shows the best fit regression line (*solid line*) along with 1-WSE limits (*dashed lines*)

known, synthetic hypocentral location. In the first case, two seconds after the first trigger (5.03 s from the event origin), 9 stations have triggered and the location is already well constrained for early warning purposes.

In the second case, at $\Delta t = 11.76$ s, 2 s after the first event detection, the constraint on the location PDF improves further, but the PDF retains an elongated shape because of the poor azimuthal coverage of the network for this event. The event depth is only constrained by an upper bound, but the depth range includes the true value.

Real-Time Magnitude Estimation Using a Bayesian, Evolutionary Approach

Previous Related Studies The problem of magnitude estimation from early seismic signal has been previously approached and analyzed by different authors.

Nakamura [31] first proposed the correlation between the event magnitude and the characteristic period of *P*-phase defined as the ratio between the energy of the signal and its first derivative.

Allen and Kanamori [2] modified the original Nakamura method and described the correlation between the predominant period and the event magnitude for Southern California events. Lockman and Allen (2007) studied the predominant period – magnitude relations for the Pacific Northwest and Japan. They also investigated the sensitivity of such relations using different frequency bands.

Using a complementary approach, Wu and Kanamori [45] investigated the feasibility of an on-site EEWS for Taiwan region based on prediction of earthquake damage, based on measurements of the predominant period and peak displacement on early *P*-wave signals detected at the network.

Odaka et al. (2003) proposed a single station approach for the real-time magnitude estimation. The authors fit the initial part of waveform envelope and showed a relation between the final event magnitude, the envelope shape coefficient and the maximum *P* amplitude measured in a 3 s time window.

Wu and Zhao [46] and Zollo et al. [49] (Fig. 11) demonstrated the existence of a correlation between the event magnitude and the peak displacement measured a few seconds after the *P* arrival based on massive analysis of Southern Californian and Euro–Mediterranean earthquake records. In particular, Zollo et al. showed that both *P* and *S* wave early phases have the potential for real time estimation of magnitude up to about *M* 7. Zollo et al. [50] and Lancieri and Zollo [26] extended this observation to Japanese earthquake records, showing that a possible saturation effect may exist at about *M* 6.5 for *P* measurements in 2 s windows while it vanishes when a larger, 4 s window is considered. The scaling of displacement peak with magnitude, instead, appears at even shorter (1 s) time lapses after the first *S*-arrival.

Using an alternative method, Simmons [38] proposed a new algorithm based on discrete wavelet transforms able to detect first *P* arrival and to estimate final magnitude analyzing first seconds of *P*-wave.

The Real-Time Magnitude Estimation Method The real time and evolutionary algorithm for magnitude estimation presented in this paper is based on a magnitude predictive model and a Bayesian formulation. It is aimed at evaluating the conditional probability density function of magnitude as a function of ground motion quantities measured on the early part of the acquired signals [19].

The predictive models are empirical relationships which correlate the final event magnitude with the logarithm of quantities measured on first 2–4 s of record.

The first prediction model, based on the predominant period of *P*-phase (τ_P), has been introduced by Allen and Kanamori [2]. Recently, Wu and Zhao [46] showed the existence of a correlation between magnitude, distance and peak displacement measured in a 2–4 s window after *P*-phase.

Zollo et al. [49,50] refined this correlation and extended the observation on the peaks measured in 2 s after the *S*-phase arrival through the analysis of the European and Japanese strong motion data-bases (Ambraseys et al. [3], K-NET www service of NIED – National Research Institute for Earth Science and Disaster Prevention, Japan).

The method therefore assumes that the linear relationship between the logarithm of the observed quantity and magnitude is known, along with standard errors of the predictive models.

At each time step t from the first station trigger, the conditional PDF of magnitude M given the observed data vector $\underline{d} = \{d_1, d_2, \ldots, d_n\}$ is expressed via the Bayes theorem as:

$$f(m|\underline{d}) = \frac{f(\underline{d}|m)f(m)}{\int_{M_{\mathrm{MIN}}}^{M_{\mathrm{MAX}}} f(\underline{d}|m)f(m)\mathrm{d}M} , \tag{7}$$

where $f(m)$ is the a priori distribution which incorporates the information available before the experimental data are collected through a truncated exponential functional form, derived by the Gutenberg–Richter recurrence relationship,

$$f(m) : \begin{cases} \frac{\beta \mathrm{e}^{-\beta m}}{\mathrm{e}^{-\beta M_{\min}} - \mathrm{e}^{-\beta M_{\max}}} & M_{\min} \le m \le M_{\max} \\ 0 & m \notin [M_{\min}, M_{\max}] \end{cases} , \tag{8}$$

where $\{\beta, M_{\min}, M_{\max}\}$ depend on the seismic features and on the detection threshold of the seismic network of the considered region.

The conditional probability $f(\underline{d}|m)$ contains all the information concerning the magnitude as retrievable from the data acquired at time t.

Assuming that components of the observed data vector $\underline{d}$ have a lognormal distribution, and that they are stochastically independent and identically distributed random variables of parameters $\mu_{\log(d)}$ and $\sigma_{\log(d)}$, then the likelihood is written as:

$$f(\underline{d}|m) = \prod_{i=1}^{\nu} \frac{1}{\sqrt{2\pi}\sigma_{\log(d)} d_i} \mathrm{e}^{-\frac{1}{2}\left(\frac{\log(d_i)-\mu_{\log(d)}}{\sigma_{\log(d)}}\right)^2} , \tag{9}$$

where ν is the number of stations acquiring at the instant t; $\mu_{\log(d)}$ and $\sigma_{\log(d)}$ are the mean and the standard deviation of the logs of d_i, respectively..

Substituting Eq. 8 and Eq. 9 into Eq. 7, $f(m|\underline{d})$ results as in Eq. 10 where it depends on data only trough $\sum_{i=1}^{\nu} \log(d_i)$ and ν, which therefore are jointly sufficient statistics for the estimation of magnitude [21]:

$$\begin{aligned} f(m|\underline{d}) &= f\left(m|\sum_{i=1}^{\nu}\log(d_i)\right) \\ &= \frac{\mathrm{e}^{\left(2\mu_{\log(d)}\left(\sum_{i=1}^{\nu}\log(d_i)\right)-\nu\mu_{\log(d)}^2\right)\Big/2\sigma_{\log(d)}^2} \mathrm{e}^{-\beta m}}{\int_{M_{\mathrm{MIN}}}^{M_{\mathrm{MAX}}} \mathrm{e}^{\left(2\mu_{\log(d)}\left(\sum_{i=1}^{\nu}\log(d_i)\right)-\nu\mu_{\log(d)}^2\right)\Big/2\sigma_{\log(d)}^2} \mathrm{e}^{-\beta m}\mathrm{d}M} . \end{aligned} \tag{10}$$

As just outlined, $f(m|\underline{d})$ depends on $\sum_{i=1}^{\nu} \log(d_i)$ and on the number of stations triggered, ν, at the time of the estimation and, consequently, on the amount of information available. As more stations are triggered, and provide more measures of d, the estimation improves.

The described technique is evolutionary in the sense that $f(m|\underline{d})$ depends on time, i. e., as time passes, additional stations provide new observations (predominant period and/or *P*-, *S*-peaks), which are used to refine the probabilistic estimation of magnitude.

Magnitude Estimation from Peak Displacement Measurements

The empirical relationships between low-pass filtered, initial *P*- and *S*-peak displacement amplitudes and moment magnitude (e. g. [49]) can be used as predictive models for the real-time estimation of magnitude using the Bayesian approach described above.

While the *P*-wave onset is identified by an automatic picking procedure, the *S*-onset can be estimated from an automatic *S*-picking or from a theoretical prediction based on the hypocentral distance given by the actual earthquake location. At a given time step after the first *P*-wave detection at the network, progressively refined estimates of magnitude are obtained from *P*- and *S*-peak displacement data. These are preliminarily corrected for distance amplitude effects through an empirical attenuation relationship obtained from available strong motion records [46,49]:

$$f(M, R) = A_{\mathrm{phase}} + B_{\mathrm{phase}} M + C_{\mathrm{phase}} \log(R) , \tag{11}$$

where the constants A_{phase}, B_{phase} and C_{phase} are determined through a best-fit regression with a retrieved standard error of $SE_{\mathrm{phase}}^{\mathrm{PMR}}$ and R is the hypocentral distance.

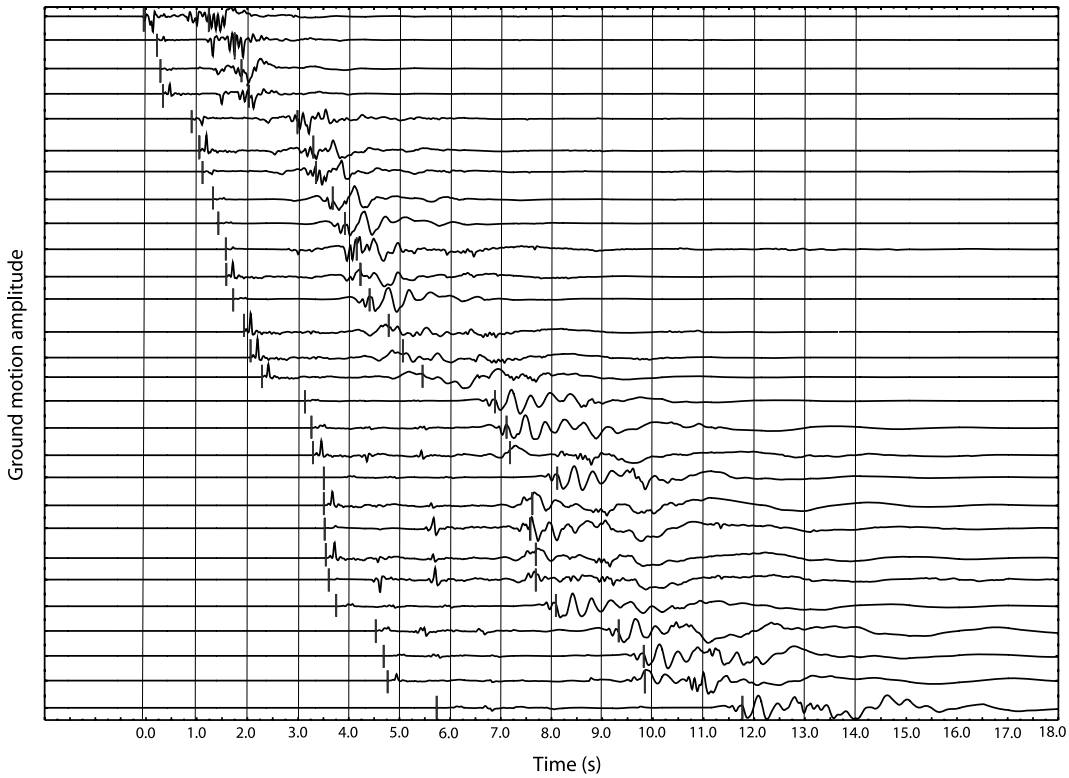

Earthquake Early Warning System in Southern Italy, Figure 12
Synthetic seismograms for a *M* 7.0 earthquake at the center of the network (see Fig. 9). The seismograms are computed using a line source, rupture model (constant rupture velocity) while complete wavefield green's functions in a flat-layered model are computed by using the discrete wavenumber summation method of Bouchon [8]. Each *vertical line* indicates the 1 s signal packets examined at each time step. This plot allows us to understand seconds after seconds which stations are acquiring and what sort of input (*P* or *S* peak) they are giving to the real time system. For example after three seconds to the first *P* phase picking thirteen stations are acquiring, the 2 s *S*-phase peak is available at the nearest stations. This observation motivates the use of the *S* phase information in a real time information. If a dense network is deployed in the epicentral area the nearest station will record the *S*-phase before the *P* phase arrives to the far ones, as seen in previous example, and this is perfectly compatible with the real time analysis

Following the procedure described in [49], the relationship (11) is used to correct observed peaks for the distance effect, by normalizing them to a reference distance (e. g., $R = 10\,\mathrm{km}$) and to determine a new best fit regression between the distance corrected peak value $(PD_{\mathrm{phase}})^{10\,\mathrm{km}}$ and the final magnitude:

$$\log\left(PD^{10\,\mathrm{km}}_{\mathrm{phase}}\right) = \log\left(PD^{R}_{\mathrm{phase}}\right) - C_{\mathrm{phase}}\log\left(\frac{R}{10}\right) \quad (12)$$

$$\log\left(PD^{10\,\mathrm{km}}_{\mathrm{phase}}\right) = A'_{\mathrm{phase}} + B'_{\mathrm{phase}}M\,. \quad (13)$$

Assuming a standard error of SE^{PM}_{phase} on peak displacements retrieved from (13) and combining the Eqs. (11) and (13), the mean values and standard deviation of quantity $\log(PD_{\mathrm{phase}})$, can be written as:

$$\begin{aligned}\mu_{\log(PD_{\mathrm{phase}})} &= B'_{\mathrm{phase}}M + A'_{\mathrm{phase}} + C_{\mathrm{phase}}\log\left(\frac{R}{10}\right)\\ \sigma_{\log(PD_{\mathrm{phase}})} &= SE^{PM}_{\mathrm{phase}} + \log\left(\frac{R}{10}\right)\Delta C_{\mathrm{phase}}\\ &\quad + C_{\mathrm{phase}}\frac{1}{R}\Delta R\,,\end{aligned} \quad (14)$$

where R is estimated with an error of ΔR and $\Delta C_{\mathrm{phase}}$ is the error on the C_{phase} coefficient in Eq. (12).

The values of coefficients in (14) used for real time magnitude estimates at ISNet are obtained from the regression analysis based on records from the European Strong Motion Database [49] and given in Table 2.

Figure 12 illustrates an example of real time magnitude estimation on a simulated event with $M = 7.0$, whose epicenter is located along the 1980 Irpinia earthquake faulting

Earthquake Early Warning System in Southern Italy, Table 2
Coefficients of the empirical regression relationships between low-pass filtered *P* and *S* displacement peaks and magnitude

Phase	A'_{phase}	B'_{phase}	C_{phase}	SE^{PM}_{phase}	ΔC_{phase}
2P	−6.31	0.70	−1.05	0.22	0.30
2S	−5.77	0.71	−0.71	0.13	0.16

system. Synthetic seismograms have been computed by using the discrete wave-number method of Bouchon [8] and Coutant (1989) for a extended source model in a flat-layered velocity model.

Figure 13a shows the probability density function defined in Eq. (8) evaluated at each time step. Time zero is assigned to the first *P* detection at the network. As time evolves the PDF tightens around the predicted magnitude value, indicating a more refined, probabilistic estimate of magnitude.

By defining $F_t(m)$ as the cumulative PDF at time t, it is possible to estimate a magnitude range of variation $[M_{\min}; M_{\max}]$ whose limits are defined based on the shape of the $F_t(m)$ function:

$$M_{\min} : \int_{-\infty}^{M_{\min}} f_t(m|\underline{d})\mathrm{d}m = \alpha \,,$$
$$M_{\max} : \int_{-\infty}^{M_{\max}} f_t(m|\underline{d})\mathrm{d}m = 1 - \alpha \,. \tag{15}$$

For example, if we assume $\alpha = 1\%$, then $M_{\min}$ and $M_{\max}$ will be, respectively, the $F_t(m)$ evaluated at 0.01 and 0.99.

In Fig. 13b the estimates of magnitude uncertainty bounds are reported as a function of time. After three iterations (corresponding to a time of 9 s from the event origin time and 4 s after the first *P*-phase arrival at the network) the magnitude estimation converges to the true magnitude value. In fact, due to the high density of seismic station in the epicentral area, at that time most of seismic station contributes to the magnitude estimation with peaks read on *P*-phase windows (Fig. 14), while a further refinement of magnitude estimate is due to the near source *S*-wave arrivals.

Real-Time Hazard Analysis for Earthquake Early Warning

The Real-Time Hazard Determination

Using the methods previously described for estimating in real-time the event magnitude and location, it is possible to perform a real-time hazard analysis [19]. This analysis is based on the extension of classical Probabilistic Seismic Hazard Analysis (PSHA) proposed by Cornell [11] that is generally used for long-term probabilistic hazard assessment. Classical PSHA integrates data from existing seismic catalogs both in terms of magnitude, location and recorded strong ground motion values in addition to the information concerning seismogenic areas of interest (ex-

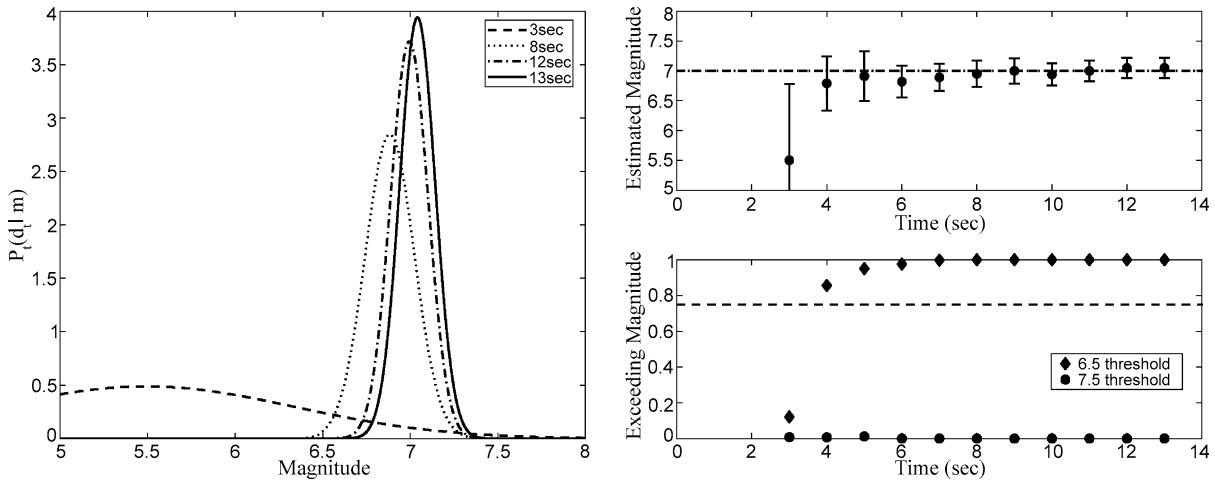

Earthquake Early Warning System in Southern Italy, Figure 13
Application of the method for real time magnitude estimate to a *M* 7 simulated event occurring within the area covered by the ISNet network. *Left panel*. PDF distribution at several time steps measured from the first *P*-phase picking. *Right top*, magnitude estimation with uncertainties as a function of time. The *dashed line* refers to the actual magnitude value, the errors represent the 95% of confidence bound evaluated as cumulative PDF integral in the 5–95% range. *Right bottom*, probability to exceed magnitude 6.5 and magnitude 7.5 thresholds in function of time. The *dashed line* is the 75% probability level

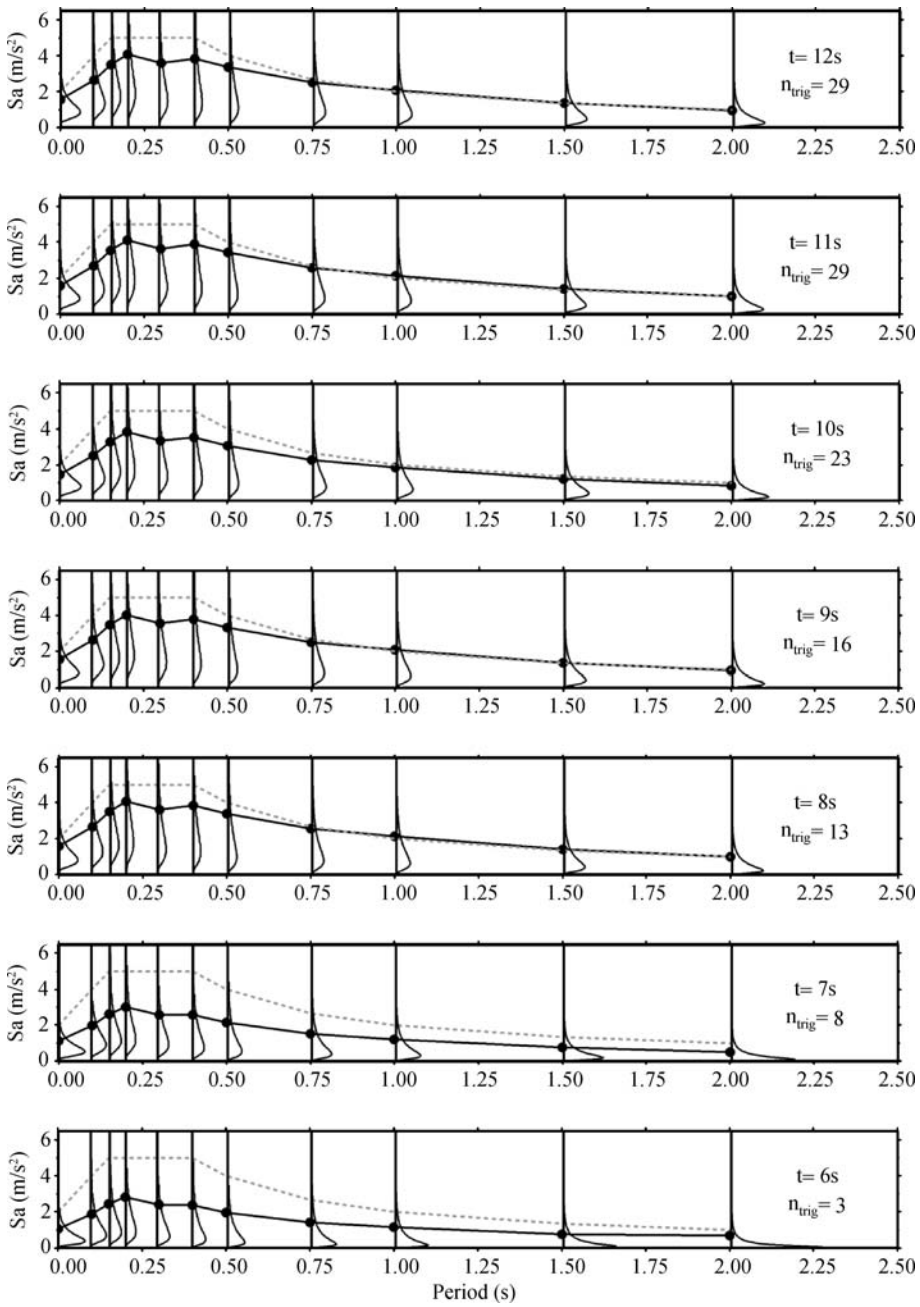

Earthquake Early Warning System in Southern Italy, Figure 14

Real-time estimation of spectral ordinates' distributions as function of the number of stations triggered for a *M* 7.0 event with an epicentral distance of 50 km from the early warning target site. The parameter n_{trig} in the figure is equivalent to the number of stations ν in the text. The acceleration spectrum (*black curve*) was obtained by choosing at each period the spectral value with 20% exceedance probability according to the corresponding distribution, so it is analogous to a uniform hazard spectrum with the exception that it is computed in real-time. The *grey dashed line* is the Italian code spectrum assigned for building design in the target location at the town of Avellino, 40 km distant from the earthquake epicenter, and is reported for comparison purposes (after [10])

pected maximum magnitude, b-value of the Gutenberg Richter relationship, etc.) to provide the hazard curve as the final outcome. Each point on that curve corresponds to the value of a ground motion intensity measure (IM) (e. g., peak ground acceleration, PGA, peak ground velocity, PGV or the spectral acceleration, Sa), having a given probability or frequency of exceedance in a fixed period of time for a site of interest.

The probabilistic framework of the PSHA, specifically the hazard integral, can be used for real-time hazard if the PDFs of magnitude and source-to-site distance are replaced with those depending on the data gathered by the EEWS during the occurrence of a specific earthquake.

This is the case, for example, of the PDF on the source-to-site distance whose statistical moments evolve with real-time earthquake location. As a consequence, this PDF does not depend on the seismic potential of the area of interest (as in the case of the classical PSHA, which accounts for the occurrence of all the earthquake in a fixed range of magnitude), but rather depends on the time evolving event location provided by the EEWS. The same considerations apply to the PDF on the magnitude as described in the following sections whose statistical moment, at a given time, depends on the number of triggered stations at that time.

In this theoretical framework the real-time hazard integral can be written as:

$$f(\mathrm{IM}|\underline{d},\underline{s}) = \int_M \int_R f(\mathrm{IM}|m,r) f(m|\underline{d}) f(r|\underline{s}) \mathrm{d}M \mathrm{d}R, \quad (16)$$

where $f(r|\underline{s})$ is the PDF of distance r, which eventually depends only on the triggering sequence of the stations in the network, where $\underline{s} = \{s_1, \ldots, s_\nu\}$ is such a sequence. This renders also the PDF of r time dependent.

Given that for each point in a volume containing the earthquake hypocenter, the probability of that point being coincident with the true hypocenter is calculated via a rapid location technique, a simple geometrical transformation allows one to obtain the probabilistic distribution of the source-to-site distance.

The PDF $f(\mathrm{IM}|m,r)$, is given, for example, by an ordinary attenuation relationship. It is worth to recall that the computed hazard refers to a particular set of triggered stations and, consequently, it depends on the information available at time t from the first detection of the event.

Figure 14 illustrates, as an example, the estimation of spectral acceleration ordinates for different periods, for a M 7.0 event located at an epicentral distance of 50 km from the early warning target site [10].

We note the evolution of Sa predictions via the corresponding PDFs. The different panels correspond to increasing times from the earthquake origin and, therefore, to different numbers of stations triggered.

The False Alarm Issue

Once the EEWS provides a probability distribution of the ground motion intensity measure (IM) at the target site (e. g., peak ground acceleration or velocity), a decisional condition has to be checked in order to decide whether to alert or not.

Several options are available to formulate a decisional rule, for example the alarm may be issued if the probability of the predicted IM exceeding a critical threshold ($\mathrm{IM_C}$) is greater than a reference value (P_c):

$$\text{Alarm if}: \int_0^{\mathrm{IM_C}} f(\mathrm{IM}|\underline{d},\underline{s}) d(\mathrm{IM}) = P[\mathrm{IM} > \mathrm{IM_C}] > P_c \,. \quad (17)$$

The efficiency of the decisional rule may be evaluated in terms of false and missed alarms probabilities (known as the "cry wolf" issue, e. g., [20]). The false alarm occurs when, on the basis of the information processed by the EEWS, the alarm is issued while the intensity measure at the site $\mathrm{IM_T}$ (T subscript means "true", indicating the realization of the IM to be distinguished from the prediction $\mathrm{IM_C}$) is smaller than the threshold $\mathrm{IM_C}$. A missed alarm corresponds to not launching the alarm if needed,

$$\begin{aligned} &\text{Missed Alarm}: \{\text{No Alarm} \cap \mathrm{IM_T} > \mathrm{IM_C}\} \\ &\text{False Alarm}: \{\text{Alarm} \cap \mathrm{IM_T} \leq \mathrm{IM_C}\} \,. \end{aligned} \quad (18)$$

It has been discussed above how the information and the uncertainties on earthquake location and magnitude are dependent on the number of stations triggered at a certain time.

Therefore, in principle, the decisional rule may be checked at any time after the first station has triggered and, consequently, the false and missed alarm probabilities are also time dependent.

Using the decisional rule of (18) and considering PGA as IM, the time evolution of false/missed alarm probabilities has been simulated for the Campania EEWS, given the occurrence of a M 7 earthquake, and a target site at an epicentral distance of 110 km.

Figure 15 reports the missed and false alarm probabilities as a function of time from the first trigger at the ISNet network.

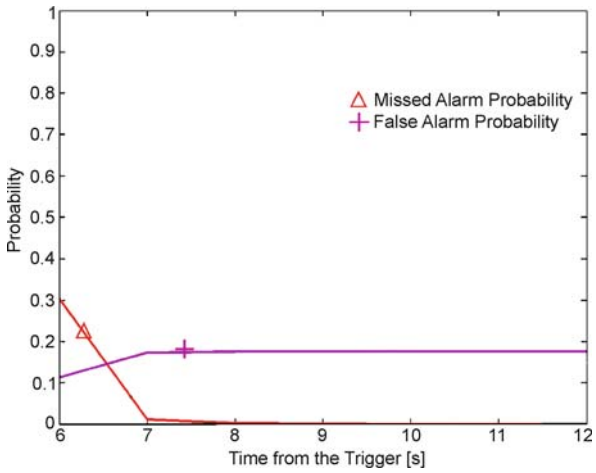

Earthquake Early Warning System in Southern Italy, Figure 15
Example of estimation of false and missed alarm probabilities as function of the time from the first trigger for a *M* 7.0 event with an epicentral distance of 110 km from the early warning target site. For the decisional rule adopted in this case the threshold is PGAc = 0.3 m/s^2 and the limit probability is $P_c = 0.2$ (after [19])

A Loss Estimation Approach to Early Warning

Magnitude and distance distributions conditioned to the measurements of the seismic network can also be used for a real-time estimation of risk, which includes losses produced by the earthquake [21]. Based on the real-time risk assessment, a security action aimed at risk mitigation is undertaken if the alarm is issued.

For example, some critical system could shut down or people in buildings may shelter themselves if the warning time is not sufficient to evacuate the dangerous buildings. More complex security measures may be related to the semi-active control of buildings [22].

Therefore, if an EEWS exists, it may trigger a security procedure in case of warning. The estimation of the expected losses for a specific building may be computed, for the case of warning issued and not issued respectively:

$$E^W[L|\underline{d},\underline{s}] = \int_L \int_{DM} \int_{EDP} \int_{IM} l f^W(l|dm) f(dm|edp) \times f(edp|im) f(im|\underline{d},\underline{s}) \mathrm{d}L\mathrm{d}DM\mathrm{d}EDP\mathrm{d}IM\,, \quad (19)$$

where $f^W(l|dm)$ is the PDF of the loss (L) given the structural and non-structural damage vector (DM) reflecting the risk reduction in the case of warning; and $f^W(l|dm)$ is the loss function if no alarm is issued (no security action is undertaken); $f(dm|edp)$ is the joint PDF of damages given the Engineering Demand Parameters (EDP), proxy for the structural response; $f(edp|im)$ is the joint PDF of the EDPs conditioned to a vector of ground motion intensity measures (IM); $f(im|\underline{d},\underline{s})$ is the real-time hazard expressed by (16) in the case of a scalar IM.

Being able to compute, before the ground motion hits the site, the expected losses in case of warning *(W)* or not ($\bar{W}$), is relevant for taking the optimal decision, i. e., to alarm if this reduces the expected losses and to not issue any warning otherwise:

$$\text{Optimal decision:} \quad \begin{array}{c} \text{to alarm if } E^W[L|\underline{d},\underline{s}] \le E^{\bar{W}}[L|\underline{d},\underline{s}] \\ \text{to not alarm if } E^W[L|\underline{d},\underline{s}] > E^{\bar{W}}[L|\underline{d},\underline{s}] \end{array} \quad (20)$$

which is a better decisional rule in respect to that of (18).

Computing and comparing expected losses, conditioned to the real-time information coming from the EEWS, in the case of alarming or not, allows the determination of the alarm threshold above which it is convenient to issue the warning according to the optimally maximum criterion.

Assessment of average loss reduction determined by issuing an Early Warning provides a quantitative tool to evaluate the efficiency and feasibility of an EEWS.

Other potential advantages given by this approach are that: (a) the threshold may be set on a statistic (i. e., the summation of the logs) inferred from seismic network measurements, dramatically reducing the required computational effort for real-time decision making; (b) it minimizes the cry wolf issue reducing the probability of false and missed alarms thanks to threshold optimization. In fact, although the number of MA and FA depend on the decisional rule adopted to issued the alarm, the approach developed in Iervolino et al. [20,21,22] avoids explicitly considering the missed and false alarm rates associated with the decision, as the choice to alarm or not is taken based on the expected economic loss (not on the estimation of peak ground motion). In other words, if in computing the expected loss one accounts for the costs of false and missed alarms, there is no need to optimize the *cry wolf* issue, and MA and FA rates are at their values determined by the respective costs, and in this sense are optimal.

Future Directions

We have analyzed and illustrated the main scientific and technological issues related to the implementation and management of an earthquake early warning system under development in the Campania region of southern Italy.

The system is designed for early warning alert notification at distant coastal targets based on a dense, wide-dynamic seismic network (accelerometers, seismometers

and broadband sensors) deployed in the Apenninic belt region (ISNet – Irpinia Seismic Network). It can therefore be classified as a regional Early Warning System consisting of a wide seismic sensor network covering a portion or the entire area which is threatened by a quake's strike.

According to [25], real-time estimates of earthquake location and magnitude are needed for regional warning systems (EEWS), i. e., dense seismic networks covering all or a portion of an area of interest. However the alarm decision in an early warning system is based, rather, on the prediction, with quantified confidence, of a ground motion intensity at a distant target site (where a sensitive structure is located). This problem needs an evolutionary (i. e., time-dependent) and probabilistic frame where pdfs for earthquake location, magnitude and attenuation parameters are combined to perform a real-time probabilistic seismic hazard analysis (e. g., [19]).

Considering the peak displacement amplitude and/or predominant frequency measured in the early portion of *P*-waves, we have shown that suitable probability density functions for the earthquake location and magnitude parameters can be constructed and used for real-time probabilistic assessment of false alarms and loss estimation, which are the key elements based on which automatic actions can be undertaken to mitigate earthquake effects.

Based on the analysis of acceleration records of Euro-Mediterranean and Japanese earthquakes, Zollo et al. [49,50] have shown the advantages of using near source strong motion records for real time estimation of earthquake magnitude. In fact they provide unsaturated recordings of moderate to large earthquakes and, in case of dense station coverage of the source area, the combination of both *P*- and *S*-wave amplitude information can be used to get fast and robust earthquake location and magnitude estimates.

We support the use of *S*-waves recorded in the near-source of an impending earthquake for earthquake early warning, especially in view of the excellent correlation that *S*-peaks show with magnitude up to about $M = 7$ for Euro-Mediterranean and Japanese earthquakes [49,50]. Dense accelerometric networks now operating in Europe, USA, Taiwan, Japan and other seismic regions in the world can provide a sufficient number of records at distances smaller than 20–30 km from potentially damaging crustal earthquakes so that *S*–*P* times are expected to be smaller than 2–3 s. A magnitude estimation using *S*-waves could be therefore available 4–5 s after the first *P*-wave is recorded, which is still useful for sending an alert to distant target sites.

Although relatively few magnitude 7 and larger earthquakes have hit the Apenninic belt, and generally the Mediterranean region, during the last century, there have been many instances of damaging quakes in the magnitude 6 range.

Earthquake early warning systems have the potential to mitigate the effects of moderate size earthquakes ($M = 6$–7), which can produce severe damage in densely urbanized areas and places where old structures were not built to current standards. This has been the case for a significant number of earthquakes occurred in the Mediterranean basin during last decades: the 1976 Friuli ($M = 6$–6.5) and 1997 Colfiorito ($M = 6$) in Italy, 1999 Athens ($M = 5.9$) in Greece, 2002 Nahrin, in Afghanistan ($M = 6.1$), 2003 in Algeria ($M = 6.7$), 2003 Bam ($M = 6.3$) in Iran, 2004 in Morocco ($M = 6.4$).

An earthquake early warning system can be effective for mitigating the effects of moderate earthquakes. For moderate size events, early warning systems could also mitigate earthquake effects in terms of infrastructure operability (e. g., hospitals, firehouses, telecommunication hubs, . . .) during the post-event emergency phase and rescue operations. For instance, in tall buildings, the higher floors generally sway much more than those near ground level, so that even a moderate earthquake could cause severe damage to a high rise. Therefore, even at 70–80 km distance from its epicenter, a magnitude 6 quake could affect hospital operating rooms and other critical installations.

Installations as close as 50 km from the epicenter could receive an earthquake warning 10 s prior to the arrival of the more energetic waves (*S* and surface waves) of an earthquake. To take advantage of this brief warning period, automated systems would have to be created that respond instantly to notification alert signals, and they would have to be carefully calibrated to avoid false or missed alarms. Closer to the epicenter, a magnitude 6 or higher earthquake can damage critical infrastructures, such as telephone lines, gas pipelines, highways, and railroads, as well as airport runways and navigation systems. These disruptions would have a domino effect in more distant areas, which could be mitigated by an early warning alert system, based on the earliest primary wave data to arrive at recording stations close to the epicenter.

Finally, we note that earthquake early warning systems can also help mitigate the effects of such earthquake-induced disasters as fires, explosions, landslides, and tsunamis, which can in many cases be more devastating than the earthquake itself. Systems could be installed at relatively low cost in developing countries, where moderate sized earthquakes can cause damage comparable to that caused by much larger earthquakes in developed countries.

Bibliography

Primary Literature

1. Allen RM (2007) The ElarmS earthquake early warning methodology and its application across California. In: Gasparini P, Manfredi G, Zschau J (eds) Earthquake early warning systems. Springer, Berlin, pp 21–44. ISBN-13 978-3-540-72240-3
2. Allen RM, Kanamori H (2003) The potential for earthquake early warning in Southern California. Science 300:786–789. doi:10.1126/science.1080912
3. Ambraseys N, Smit P, Douglas J, Margaris B, Sigbjornsson R, Olafsson S, Suhadolc P, Costa G (2004) Internet site for European strong-motion data. Boll Geofis Teor Appl 45(3):113–129
4. Bakun W, Fischer HF, Jensen E, VanSchaack J (1994) Early warning system for aftershocks. Bull Seismol Soc Am 84(2):359–365
5. Bernard P, Zollo A (1989) The Irpinia (Italy) 1980 earthquake: detailed analysis of a complex normal fault. J Geophys Res 94:1631–1648
6. Guidoboni E, Ferrari G, Mariotti D, Comastri A, Tarabusi G, Valensise G (2007) CFTI4Med, Catalogue of Strong Earthquakes in Italy (461 B.C.-1997) and Mediterranean Area (760 B.C.-1500). INGV-SGA. Available from http://storing.ingv.it/cfti4med/
7. Bose M, Ionescu C, Wenzel F (2007) Earthquake early warning for Bucharest, Romania: Novel and revised scaling relations. Geophys Res Lett 34:L07302. doi:10.1029/2007GL029396
8. Bouchon M (1979) Discrete wave number representation of elastic wave fields in three-space dimensions, J Geophys Res 84:3609–3614
9. Cinti FR, Faenza L, Marzocchi W, Montone P (2004) Probability map of the next $M \geq 5.5$ earthquakes in Italy. Geochem Geophys Geosyst 5:Q1103. doi:10.1029/2004GC000724.
10. Convertito V, Iervolino I, Giorgio M, Manfredi G, Zollo A (2008) Prediction of response spectra via real-time earthquake measurements. Soil Dyn Earthq Eng 28(6):492–505. doi:10.1016/j.soildyn.2007.07.006
11. Cornell CA (1968) Engineering seismic hazard analysis. Bull Seismol Soc Am 59(5):1583–1606
12. Cua G, Heaton T (2007) The virtual seismologist (VS) method: A Bayesian approach to earthquake early warning. In: Gasparini P, Manfredi G, Zschau J (eds) Earthquake early warning systems. Springer, Berlin. doi:10.1007/978-3-540-72241-0_7
13. Curtis A, Lomax A (2001) Prior information, sampling distributions and the curse of dimensionality. Geophysics 66:372–378. doi:10.1190/1.1444928
14. Erdik M, Fahjan Y, Ozel O, Alcik H, Mert A, Gul M (2003) Istanbul earthquake rapid response and the early warning system. Bull Earthquake Eng 1(1):157–163. doi:10.1023/A:1024813612271
15. Espinosa-Aranda JM, Jimenez A, Ibarrola G, Alcantar F, Aguilar A, Inostroza M, Maldonado S (1995) Mexico City seismic alert system. Seismol Res Lett 66:42–53
16. Font Y, Kao H, Lallemand S, Liu C-S, Chiao L-Y (2004) Hypocentral determination offshore Eastern Taiwan using the maximum intersection method. Geophys J Int 158(2):655–675. doi:10.1111/j.1365-246X.2004.02317.x
17. Grasso V, Allen RM (2005) Earthquake warning systems: Characterizing prediction uncertainty. Eos Trans AGU 86(52), Fall Meet. Suppl., Abstract S44B-03
18. Horiuchi S, Negishi H, Abe K, Kamimura A, Fujinawa Y (2005) An automatic processing system for broadcasting earthquake alarms. Bull Seism Soc Am 95(2):708–718. doi:10.1785/0120030133
19. Iervolino I, Convertito V, Giorgio M, Manfredi G, Zollo A (2006) Real time risk analysis for hybrid earthquake early warning systems. J Earthq Eng 10(6):867–885
20. Iervolino I, Convertito V, Giorgio M, Manfredi G, Zollo A (2007a) The cry wolf issue in seismic early warning applications for the campania region. In: Gasparini P et al (eds) Earthquake early warning systems. Springer, Berlin. doi:10.1007/978-3-540-72241-0_11
21. Iervolino I, Giorgio M, Manfredi G (2007b) Expected loss-based alarm threshold set for earthquake early warning systems. Earthq Eng Struc Dyn 36(9):1151–1168. doi:10.1002/eqe.675
22. Iervolino I, Manfredi G, Cosenza E (2007c) Earthquake early warning and engineering applications prospects. In: Gasparini P, Manfredi G, Szchau J (eds) Earthquake early warning systems. Springer, Berlin, doi:10.1007/978-3-540-72241-0_12
23. Jenny S, Goes S, Giardini D, Kahle H-G (2006) Seismic potential of Southern Italy. Tectonophysics 415:81–101. doi:10.1016/j.tecto.2005.12.003.
24. Kamigaichi O (2004) JMA earthquake early warning. J Japan Assoc Earthq Eng 3:134—137
25. Kanamori H (2005) Real-time seismology and earthquake damage mitigation. Ann Rev Earth Planet Sci 33:195–214. doi:10.1146/annurev.earth.33.092203.122626
26. Lancieri M, Zollo A (2008) A bayesian approach to the real-time estimation of magnitude from the early *P*- and *S*-wave displacement peaks. J Geophys Res. doi:10.1029/2007JB005386, in press
27. Lomax A (2005) A Reanalysis of the hypocentral location and related observations for the great 1906 California earthquake. Bull Seism Soc Am 95(3):861–877. doi:10.1785/0120040141
28. Meletti C, Patacca E, Scandone P (2000) Construction of a seismotectonic model: The case of Italy. Pure Appl Geophys 157:11–35
29. Montone P, Mariucci MT, Pondrelli S, Amato A (2004) An improved stress map for Italy and surrounding regions (central Mediterranean). J Geophys Res 109:B10410. doi:10.1029/2003JB002703
30. Munich Re (eds) (2005) Environmental report – perspectives – Today's ideas for tomorrow's world, WKD-Offsetdruck GmbH, München
31. Nakamura Y (1988) On the urgent earthquake detection and alarm system (UrEDAS). Proc 9th World Conf Earthquake Eng VII, Toyko, 673–678
32. Nakamura Y (1989) Earthquake alarm system for Japan railways. Japan Railway Eng 109:1–7
33. Nakamura Y (2004) Uredas, urgent earthquake detection and alarm system, now and future. 13th World Conference on Earthquake Engineering 908
34. Okada T et al (2003) A new method of quickly estimating epicentral distance and magnitude from a single seismic record. Bull Seismol Soc Am 93(1):526–532. doi:10.1785/0120020008
35. Podvin P, Lecomte I (1991) Finite difference computations of traveltimes in very contrasted velocity models: a massively parallel approach and its associated tools. Geophys. J Int. 105:271–284

36. Rydelek P, Pujol J (2004) Real-time seismic warning with a 2-station subarray, Bull Seism Soc Am 94(4):1546–1550. doi:10.1785/012003197
37. Satriano C, Lomax A, Zollo A (2008) Real-time evolutionary earthquake location for seismic early warning. Bull Seism Soc Am 98(3):1482–1494. doi:10.1785/0120060159
38. Simons F, Dando JB, Allen R (2006) Automatic detection and rapid determination of earthquake magnitude by wavelet multiscale analysis of the primary arrival. Earth Planet Sci Lett 250:214–223. doi:10.1016/j.epsl.2006.07.039
39. Teng TL, Wu Y-M, Shin TC, Tsai YB, Lee WHK (1997) One minute after: strong-motion map, effective epicenter, and effective magnitude. Bull Seism Soc Am 87(5):1209–1219
40. Tsukada S (2006) Earthquake early warning system in Japan. Proc 6th Joint Meeting UJNR Panel on Earthquake Research, Tokushima, Japan
41. Valensise G, Amato A, Montone P, Pantosti D (2003) Earthquakes in Italy: Past, present and future. Episodes 26(3):245–249
42. Wenzel FM et al (1999) An early warning system for Bucharest. Seismol Res Lett 70(2):161–169
43. Westaway R, Jackson J (1987) The earthquake of 1980 November 23 in Campania-Basilicata (southern Italy), Geophys J R Astron Soc 90:375–443. doi:10.1111/j.1467-6435.1999.tb00581.x
44. Wu Y-M, Teng T (2002) A virtual subnetwork approach to earthquake early warning. Bull Seismol Soc Am 92(5):2008–2018. doi:10.1785/0120040097
45. Wu Y-M, Kanamori H (2005) Experiment on onsite early warning method for the Taiwan early warning system. Bull Seismol Soc Am 95(1):347–353. doi:10.1785/0120040097
46. Wu YM, Zhao L (2006) Magnitude estimation using the first three seconds of *p*-wave amplitude in earthquake early warning. Geophys Res Lett 33:L16312. doi:10.1029/2006GL026871
47. Wurman G, Allen RM, Lombard P (2007) Toward earthquake early warning in Northern California. J Geophys Res 112:B08311. doi:10.1029/2006JB004830
48. Zhou H (1994) Rapid 3-D hypocentral determination using a master station method, J Geophys Res 99(B8):15439–15455
49. Zollo A, Lancieri M, Nielsen S (2006) Earthquake magnitude estimation from peak amplitudes of very early seismic signals on strong motion records. Geophys Res Lett 33:L23312. doi:10.1029/2006GL027795
50. Zollo A, Lancieri M, Nielsen S (2007) Reply to comment by P. Rydelek et al on "Earthquake magnitude estimation from peak amplitudes of very early seismic signals on strong motion records". Geophys Res Lett 34:L20303. doi:10.1029/2007GL030560.

Books and Reviews

Berger JO (1985) Statistical decision theory and Bayesian analysis. Springer, New York
Coutant O (1989) Program de simulation numerique AXITRA. Rapport LGIT, Grenoble, France
Gruppo di Lavoro MPS (2004) Redazione della mappa di pericolosità sismica prevista dall'Ordinanza PCM 3274 del 20 marzo (2003) Rapporto Conclusivo per il Dipartimento della Protezione Civile, INGV, Milano-Roma, aprile (2004) 65 pp + 5 appendici
Milne J (1886) Earthquakes and other earth movements. Appelton, New York, p 361

Earthquake Engineering, Non-linear Problems in

Mihailo D. Trifunac
Department of Civil Engineering,
University of Southern California, Los Angeles, USA

Article Outline

Glossary

Meta-stability of man-made structures is the consequence of their upright construction above ground. For excessive dynamic (earthquake) loads, when the lateral deflection exceeds some critical value (this is normally accompanied by softening nonlinear behavior of the structural members), the overturning moment of the gravity forces becomes larger than the restoring moment, and the structure becomes unstable and moves exponentially toward collapse.

Complex and evolving structural systems are structures with a large number of degrees of freedom and many structural members, which for given loads experience softening nonlinear deformations. During strong excitation, continuous changes (typically decreases) in effective stiffness and time-dependent changes in boundary conditions result in a system whose properties are changing with time.

Soil–structure interaction is a process in which the soil and the structure contribute to mutual deformations while undergoing dynamic response. In time, with continuously changing contact area between the foundation and the soil (opening and closing of gaps), when the deformations are large, soil–structure interaction is characterized by nonlinear geometry and nonlinear material properties in both the soil and in the structure.

Definition of the Subject

Nonlinear problems in structural earthquake engineering deal with the dynamic response of meta-stable, man-